



Cost-based optimum design of the earthquake-resistant system for continuous skew overpasses

Penghui Zhang, Wancheng Yuan, Zhiqiang Wang, Hongya Qu^{*}

Dept. of Bridge Engineering, Tongji Univ., 1239 Siping Rd., Shanghai 200092, China

ARTICLE INFO

Keywords:
 Seismic design optimization
 Skew bridge
 Repair cost estimation
 Probabilistic seismic demand model
 Response surface method

ABSTRACT

This study proposes an efficient optimization framework for the earthquake-resistance system of continuous skew overpasses based on a cost-related objective function. The cable-sliding modular expansion joint (CMEJ) was considered to mitigate the rotational response of skew bridges. The BOX-COX regression was used to modify the probabilistic seismic demand model (PSDM) so that assumptions of the cloud method, viz. linearity, normality, and homoscedasticity, can be satisfied. The optimal intensity measure (IM) was selected from ten candidates. Next, the size of laminated rubber bearings (LRBs) and the initial free movement displacement of joints were optimized through the response surface method (RSM) and the Particle Swarm Optimization (PSO). Finally, the proposed framework was demonstrated using a typical three-span skew continuous overpass bridge. The seismic mitigation effectiveness of the CMEJ was discussed, considering the impact of the skew angle. Results indicate that the proposed optimization method can efficiently minimize the cost-related objective function with acceptable accuracy. Additionally, compared to the bridge equipped with modular expansion joints (MEJs), bearings of the bridge equipped with CMEJs have a smaller damage probability while the damage probability of abutments increases, which results in the total expected repair cost decreases obviously. It is also notable that the total expected repair cost of the bridge with MEJs increases as the skew angle becomes more extensive, while the one for the bridge with CMEJs is independent of the skew angle.

1. Introduction

Skew bridges are commonly used in overpasses of highway intersections or interchanges due to their adaptability of alignment. Bridge-abutment interaction is more prominent in skew bridges under strong earthquakes, which leads to excessive in-plane rotation and unseating at the acute corners of abutments [1–3]. In order to prevent unseating of skew bridges in seismically active regions, the minimum support length has to be satisfied. The requirement of support length was investigated by several researchers considering the effects of different ground motion types (e.g., far-field ground motions and near-field ground motions) and bridge geometries (e.g., skew angle, span width, and the number of spans) [4–7]. However, the demand for support length will be extremely great as far as severe earthquakes are considered, which is of economic concern. Therefore, it is necessary to propose seismic mitigation approaches for skew bridges located in high seismic zones. Link slabs were adopted to retrofit multi-simple-span skew bridges by Sevgili and Caner [8]. As a result, the transverse and longitudinal displacements, as well as the substructure seismic forces, were

reduced. Cable restrainers were also used to decrease the rotation of skew bridge decks, and the design method for simply-supported bridges was developed [9,10]. Nevertheless, cable restrainers have certain limitations, such as increased bearing reaction force and lack of design procedure for continuous skew bridges. In this regard, modular expansion joints combined with cable restrainers, named cable-sliding modular expansion joints (CMEJs), were used to overcome the limitations, and the seismic mitigation effectiveness for skew overpasses was verified by seismic fragility analysis [11–13]. Moreover, it is also necessary to set up an optimization framework to determine the optimum design parameters for skew continuous overpasses.

Selecting optimal design parameters for structures can improve the seismic performance of structures without significantly increasing construction costs. The conventional trial-and-error design procedure is often used, but its efficiency and accuracy are limited when the number of design parameters is more than three [14]. To address this issue, researchers have made intensive efforts to determine optimal design parameters for structures by using various heuristic algorithms, such as harmony search [15], genetic algorithm [16], simulated annealing

* Corresponding author.

E-mail addresses: penghui@tongji.edu.cn (P. Zhang), yuan@tongji.edu.cn (W. Yuan), wangzhiq@tongji.edu.cn (Z. Wang), hqu@tongji.edu.cn (H. Qu).

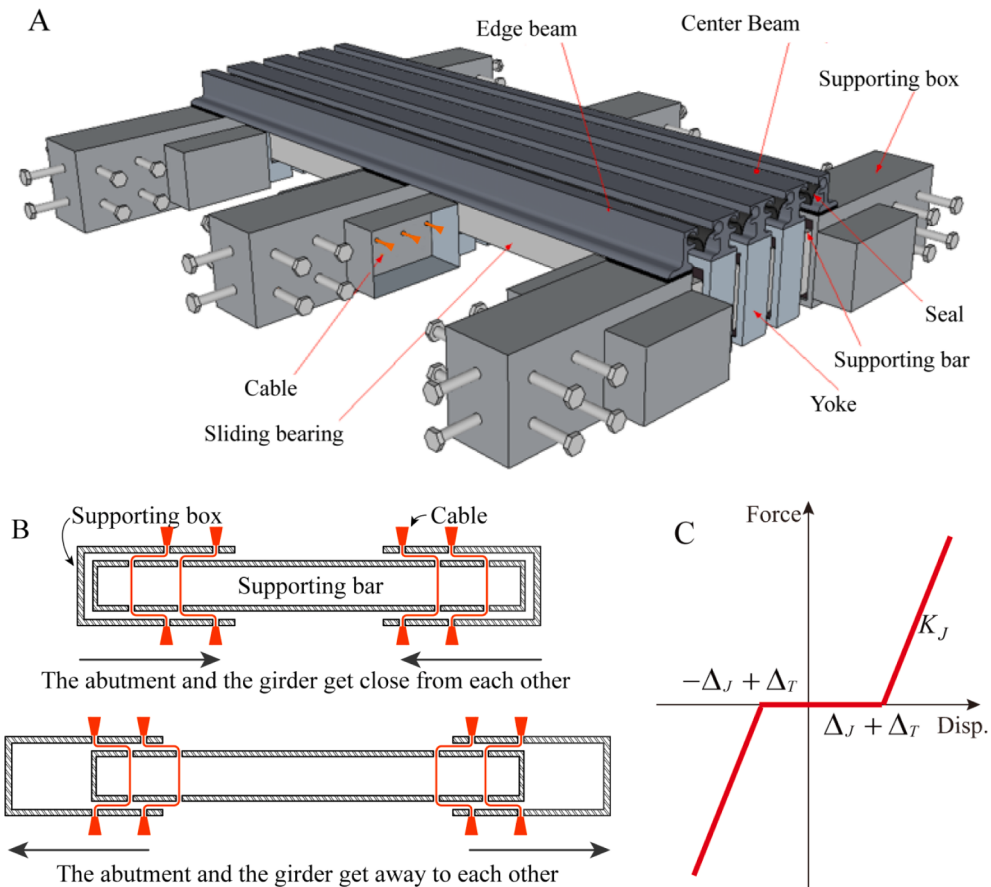


Fig. 1. Cable-sliding modular expansion joint: (A) schematic, (B) working mechanism, (C) force–displacement relationship.

algorithm [17], and bio-inspired search methods [18]. Although the aforementioned highly iterative algorithms are able to identify the optimal design parameters for simple structures, the optimum design of complicated structures (e.g., skew continuous overpasses) is still intricate since the calculation cost of the nonlinear time history analysis during every iteration is relatively expensive. Besides, appropriate performance indicators need to be considered as optimization objectives. When the seismic force/deformation response, which is commonly used in the early damage stages, is taken as the optimization objective, the optimization result varies with different ground motion records. Therefore, fragility-based [19–21], resilience-based [22], and seismic-repair-cost-based [23,24] optimization procedures are developed to consider the uncertainties of ground motions, material, and geometry. In performance-based earthquake engineering, the seismic loss is a typical decision-making indicator [25]. Seismic loss of bridges can be divided into two categories—direct and indirect losses. Indirect loss mainly includes the cost of productivity loss caused by longer travel time and consumption of additional fuel of vehicles due to the unavailability of bridges. Direct loss consists of cost from the repair of damaged structural components, which is directly related to the seismic performance of bridges. Several bridge seismic loss models have been proposed considering various repair actions and uncertainties in repair actions and costs [26–30]. However, the optimization design of an individual bridge based on direct loss and construction costs was not studied.

To estimate the life-cycle repair cost for a specific bridge, the probabilistic seismic demand model (PSDM) needs to be developed. In accordance with the PSDM, the relationship between ground motion intensity measure (IM) and engineering demand parameter (EDP) is established. Owing to its computational efficiency, the cloud method has become one of the fundamental approaches to building up the PSDM [31,32]. Nevertheless, the assumptions (i.e. normality, linearity, and

homoscedasticity) of such a method are normally inconsistent with actual outcomes [33–35]. This can be further interpreted for the following reasons: (1) EDP under a given IM does not strictly follow lognormal distribution; (2) poor linear correlation between $\ln(\text{IM})$ and $\ln(\text{EDP})$ exists in some cases, where $\ln(\cdot)$ is the natural logarithm function; (3) variance of $\ln(\text{EDP})$ varies with the change of IM. Considerable studies have focused on these three issues that exist in the cloud method. Karamlou and Bocchini [35] studied the influence of these three assumptions using analytical fragility curves with a large number of numerical analyses considering uncertainties of structural material and modeling parameters. The results implied that the first issue does not lead to significant error on the fragility curve while the others do. In terms of the second issue, most studies focused on developing or selecting an optimal IM, which retains a significant logarithmic linear relation with the EDP for specific site conditions and structure types [36–40]. To the best of the authors' knowledge, there are no studies addressing the third issue.

In this study, the CMEJ and the laminated rubber bearing (LRB) were adopted as an earthquake-resistant system for continuous skew overpasses. An improved PSDM based on BOX-COX regression was developed to satisfy the three fundamental assumptions of the cloud method. A component-based repair cost estimation framework was established in accordance with the improved PSDM. An efficient optimization procedure to determine the optimal design parameters for the earthquake-resistant system was proposed with a cost-related objective function, where the function consists of construction cost and expected seismic repair cost. A continuous skew overpass was selected as a case study, followed by optimal IM selection for the bridge. Finally, seismic mitigation effectiveness of the CMEJ was discussed, considering the impact of skew angle.

2. Cable-sliding modular expansion joint (CMEJ)

To prevent girder falling, cable restrainers are widely adopted to decrease possible excessive relative displacement between girder and substructure. Both deterministic and probabilistic analyses show that cable restrainers alter overall structural response and lower the probability of damage occurrence, when bridges are subjected to severe ground motions [41,42]. Besides steel cables, fiber-reinforced polymer (FRP) cables (with high tensile strength), and shape memory alloy (SMA) cables (with energy dissipation capacity and self-centering capability) are also used as seismic restrainers. It was found that CMEJ can control the relative displacement between adjacent girders, hence avoiding collision [11,12].

Design details of the CMEJ are shown in Fig. 1A. There are three supporting boxes along the transverse direction. The live load of the joint is transferred to supporting bars through center beams. The ends of the supporting box and supporting bar are connected with steel cables, which makes CMEJs distinctive from conventional modular expansion joints. Supporting boxes anchor in girders or abutments. Under minor earthquakes, temperature variation, shrinkage, and creep, the relative displacement between the supporting box and the supporting bar is less than the initial free movement displacement. The cable will not tighten, and the supporting bar moves freely in supporting boxes like conventional modular expansion joints (MEJs). Under severe earthquakes, the cable begins to tighten and keep the relative displacement between the supporting bar and the supporting box in an acceptable range so as to limit the displacement between the girder and abutments. The deformation of cables is shown in Fig. 1B when the abutment and the girder get close or away from each other. The restoring force of the cable (Fig. 1C) can be expressed as:

$$F = \begin{cases} K_J(\Delta_d - \Delta_+) & \Delta_d \geq \Delta_+ \\ K_J(\Delta_d - \Delta_-) & \Delta_d < \Delta_- \\ 0 & \Delta_- \leq \Delta_d < \Delta_+ \end{cases}, \quad \Delta_+ = \Delta_J + \Delta_T, \quad \Delta_- = -\Delta_J + \Delta_T, \quad K_J = nE_J A_J / 2L_J \quad (1)$$

where Δ_d is the relative displacement between abutment and girder, Δ_J is the initial free movement displacement between the supporting box and the supporting bar, Δ_T is the temperature-induced abutment-deck displacement, K_J is the stiffness of the CMEJ which is determined by the number of cables (n), modulus of elasticity (E_J), total section area of the cables (A_J) and length of each cable (L_J).

3. Probabilistic seismic demand model

3.1. Least squares linear regression

The simple linear regression model was adopted for response prediction when two variables (independence and response) are of significant linear correlation, as expressed in Eq. (2):

$$y = \alpha_0 + \alpha_1 x + e \quad (2)$$

where α_0 and α_1 are regression coefficients; x and y are the independence and response variables, respectively; and e is the residual error.

The ordinary least squares method (OLSM) is applied to calculate the estimated values of α_0 and α_1 by minimizing the residual sum of squares. The residual sum of squares reflects the discrepancy between actual values of y ($y_i, i = 1, 2, \dots, n$) and their predicted values are expressed as:

$$Q(\alpha_0, \alpha_1) = \sum_{i=1}^n e_i^2 = \sum_{i=1}^n (y_i - \alpha_0 - \alpha_1 x_i)^2 \quad (3)$$

Eq. (3) can also be obtained through the maximum likelihood estimation method (MLEM), which reveals the intrinsic mechanism of the OLSM. When the i -th residual error e_i is assumed to obey normal

distribution with constant variance σ^2 , the i -th observed response y_i follows the normal distribution:

$$y_i \sim N(\alpha_0 + \alpha_1 x_i, \sigma^2) \quad (4)$$

Then, the probability density function $f(y_i)$ takes the form of:

$$f(y_i) = \frac{1}{\sqrt{2\pi}\sigma} \exp\left\{-\frac{1}{2\sigma^2}[y_i - \alpha_0 - \alpha_1 x_i]^2\right\} \quad (5)$$

Finally, if observed responses are mutually independent, the likelihood function can be written as:

$$L(\alpha_0, \alpha_1) = \prod_{i=1}^n f(y_i) = (2\pi\sigma^2)^{-\frac{n}{2}} \exp\left\{-\frac{1}{2\sigma^2} \sum_{i=1}^n [y_i - \alpha_0 - \alpha_1 x_i]^2\right\} \quad (6)$$

Taking natural logarithm at both sides of Eq. (6) yields:

$$\begin{aligned} \ln(L) &= -\frac{n}{2} \ln(2\pi\sigma^2) - \frac{1}{2\sigma^2} \sum_{i=1}^n [y_i - \alpha_0 - \alpha_1 x_i]^2 \\ &= -\frac{n}{2} \ln(2\pi\sigma^2) - \frac{1}{2\sigma^2} Q(\alpha_0, \alpha_1) \end{aligned} \quad (7)$$

Therefore, maximizing the likelihood function $L(\alpha_0, \alpha_1)$ is equivalent to minimizing the residual sum of squares $Q(\alpha_0, \alpha_1)$.

Based on the aforementioned analysis, least squares linear regression relies on four fundamental assumptions: (1) significant linear correlation between variables and; (2) residual error follows the normal distribution; (3) variance of is constant; and (4) residual errors are mutually independent. All four assumptions should be satisfied in the OLSM-based cloud method, but the first three are often inconsistent with the actual outcomes of the PSDM.

3.2. BOX-COX regression

The Box-Cox regression can handle nonlinearity, non-normality, and heteroskedasticity by data transformation. It was proposed by Box and Cox in 1964, which is written as [43]:

$$y^{(\lambda)} = \begin{cases} \frac{(y+s)^\lambda - 1}{\lambda}, & \lambda \neq 0 \\ \ln(y+s), & \lambda = 0 \end{cases} \quad (8)$$

where s is the coefficient to guarantee the algebraic sum of y and s greater than zero. If $y > 0, s = 0$; otherwise $s = \text{ceil}(|\min(y)|)$, and $\text{ceil}(\cdot)$ denotes ceiling function.

Applying the BOX-COX transformation to the response variable in Eq. (1) leads to the Box-Cox regression model:

$$y^{(\lambda)} = \alpha'_0 + \alpha'_1 x + e' \quad (9)$$

The optimal value of λ is determined by the maximum likelihood estimation. Assuming e'_i is a random variable under normal distribution with zero mean and variance of σ'^2 , the joint probability density function of the residual error vector $e' = (e'_1, e'_2, \dots, e'_n)$ takes the form as:

$$f(e') = (2\pi\sigma'^2)^{-\frac{n}{2}} \exp\left\{-\frac{1}{2\sigma'^2} \sum_{i=1}^n e'^2_i\right\} \quad (10)$$

Then, the joint probability density function of the response vector $y = (y_1, y_2, \dots, y_n)$ can be written as:

$$f(y) = (2\pi\sigma'^2)^{-\frac{n}{2}} \exp\left\{-\sum_{i=1}^n \frac{[y_i^{(\lambda)} - (\alpha'_0 + \alpha'_1 x_i)]^2}{2\sigma'^2}\right\} \prod_{i=1}^n y_i^{\lambda-1} \quad (11)$$

Taking natural logarithm of Eq. (11) yields the likelihood function:

$$L(\lambda) = (\lambda - 1) \sum_{i=1}^n \ln(y_i) - \frac{n}{2} \ln\left\{\sum_{i=1}^n \frac{[y_i^{(\lambda)} - (\alpha'_0 + \alpha'_1 x_i)]^2}{n-2}\right\} \quad (12)$$

It is difficult to obtain partial derivatives for Eq. (12), therefore, the optimal numerical solution value of coefficient λ , which maximizes $L(\lambda)$, is generally set with the small searching step size of 0.01.

3.3. PSDM based on cloud method

Cornell et al. [44] found that the relationship between the mean value of EDP (S_D) and IM can be estimated using the power model:

$$S_D = aIM^b \quad (13)$$

This can be rewritten to perform the least squares linear regression model in the following form:

$$\ln(D) = a + b\ln(IM) + e, e \sim N(0, \beta_D^2) \quad (14)$$

where a and b are regression coefficients obtained using OLSM. Due to the adoption of least squares linear regression, the assumptions of normality, linearity, and homoscedasticity should be followed when the cloud method is used. The conditional probability that a bridge component (i.e., abutments, bearings, columns) experiences a certain level of demand (D) at a given IM level is defined as:

$$P[D > d|IM] = 1 - \Phi\left[\frac{\ln(d) - \ln(S_D)}{\beta_D}\right] \quad (15)$$

The logarithmic standard deviation of seismic demand is determined as:

$$\beta_D = \sqrt{\frac{\sum_{i=1}^n [\ln(D_i) - a - b\ln(IM_i)]^2}{n - 2}} \quad (16)$$

Moreover, the bridge component fragility of j -th damage state (DS_j) takes the form of Eq. (17), if the capacity (C) is also assumed to follow a lognormal distribution:

$$P[DS_j|IM] = \Phi\left[\frac{\ln(S_D) - \ln(S_C)}{\sqrt{\beta_D^2 + \beta_C^2}}\right] \quad (17)$$

where S_C and β_C are the mean and logarithmic standard deviation of C , respectively.

3.4. PSDM based on BOX-COX regression

To eliminate the influence of the first three fundamental assumptions (given in Section 3.1) of cloud method without significant increase of computational cost, a new PSDM using BOX-COX regression is proposed in this study, and Eq. (14) is updated to be:

$$\ln(D)^{(\lambda)} = a' + b'\ln(IM) + e', e' \sim N(0, \beta'_D^2) \quad (18)$$

where a' and b' are regression coefficients obtained using the ordinary least squares method. $\ln(EDP)^{(\lambda)}$, instead of $\ln(EDP)$, is a normally distributed random variable with mean of $a' + b'\ln(IM)$ and variance of β'_D^2 . As a result, the component fragility can no longer be written in a simple form of Eq. (17), and $\ln(D)^{(\lambda)}$ values (under normal distribution)

are generated using the Monte Carlo Sampling (MCS) technique instead. The number of samples is taken as 10^5 considering accuracy and efficiency of fragility analysis. $\ln(D)$ is adopted using BOX-COX inverse transformation:

$$\ln(D) = \begin{cases} \left[\lambda \ln(D)^{(\lambda)} + 1\right]^{\frac{1}{\lambda}} - s, & \lambda \neq 0 \\ \exp[\ln(D)^{(\lambda)}] - s, & \lambda = 0 \end{cases} \quad (19)$$

The indicator function is used to judge each demand-capacity sample:

$$I[\ln(D) \geq \ln(C)] = \begin{cases} 0, & \ln(D) < \ln(C) \\ 1, & \ln(D) \geq \ln(C) \end{cases} \quad (20)$$

Finally, the failure probability of the component takes the form of:

$$P[DS_j|IM] = \frac{\sum_{k=1}^{10^5} I[\ln(D_k) \geq \ln(C_k)]}{10^5} \quad (21)$$

4. Probabilistic seismic loss assessment

The expected repair cost for a given IM, $E[L_T|IM]$, was evaluated based on an extension of the repair cost estimation procedure proposed by Kameshwar and Padgett [26]. A large number ($n_s=10^5$) of MCSs were performed for each given IM. Within each simulation, the structure restoration cost was derived by summing up the repair costs for all types of bridge components. Therefore, the mean structure restoration cost with respect to the given IM can be expressed as:

$$E[L_T|IM] = \frac{1}{n_s} \sum_{p=1}^{n_s} \sum_{c=1}^{n_c} L_{c|IM}^p \quad (22)$$

where n_c refers to the number of component types. In this study, three main types of components (abutments, bearings, and piers) were considered, giving $n_c = 3$. Considering the repair cost of shear keys is comparatively negligible, and investigation of repair actions and repair costs for shear keys is inadequate, the damage of shear keys is not considered in probabilistic seismic loss assessment. $L_{c|IM}^p$ is the repair costs of all elements belonging to the component type c , and can be derived as the sum of the repair costs of various damage modes with regard to component type c , which can be given by:

$$L_{c|IM}^p = \sum_{d=1}^{n_{d|c}} L_{d|c|IM}^p \quad (23)$$

where $L_{d|c|IM}^p$ is the repair cost for component type c suffering damage mode d . In this work, the damage modes of abutments were identified by active and passive deformations (δ_a and δ_p); laminated rubber bearings (LRBs) were assumed to be damaged due to longitudinal and transverse displacements (δ_{bl} and δ_{bt}), and damage modes of piers were measured by curvature ductility (μ_c). $n_{d|c}$ refers to the number of damage modes of component type c . The component repair cost of an individual damage mode can be acquired as the sum of the repair cost of every element e belonging to the component type c :

Table 1
Component capacity models for various limit states.

EDP	Slight	Moderate	Extensive	Complete	Reference	
	S_c	β_c	S_c	β_c	S_c	β_c
$\delta_p(\text{mm})$	37.0	0.25	146	0.25	1000	0.47
$\delta_a(\text{mm})$	9.8	0.25	37.9	0.25	77.2	0.47
$\delta_{bl}(\text{m})$	Δ_f	0.25	Δ_{l1}	0.25	Δ_{l2}	0.47
$\delta_{bt}(\text{m})$	Δ_f	0.25	Δ_{r1}	0.25	Δ_{r2}	0.47
μ_c	1.00	0.08	5.12	0.09	9.24	0.10
					13.36	0.10
					/	

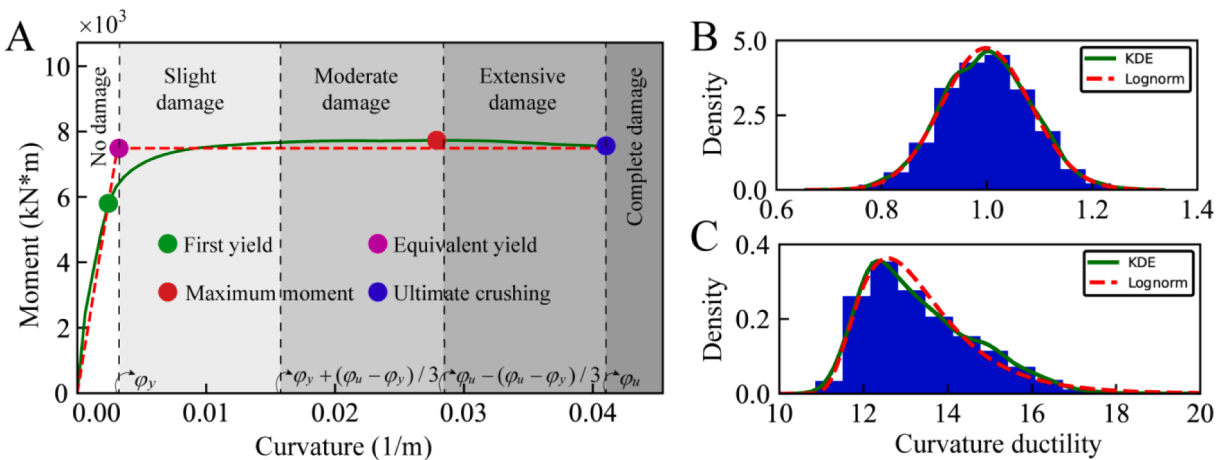


Fig. 2. Capacity model for piers: (A) definition of various limit states, (B) distribution of the curvature ductility corresponding to slight damage state, (C) distribution of the curvature ductility corresponding to complete damage state.

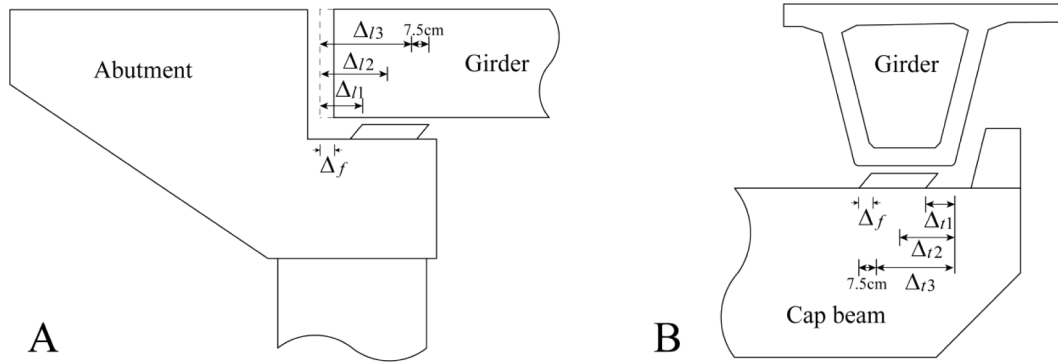


Fig. 3. limit states of LRBs: (A) longitudinal, (B) transverse.

$$L_{d|c|IM}^p = \sum_{e=1}^{n_{e|d|c}} L_{e|d|c|IM}^p \quad (24)$$

where $n_{e|d|c}$ refers to the number of elements belonging to component type c suffering the same damage mode d . The damage state of each element is determined as:

$$DS_{e|d|c|IM}^p = \sum_{l=1}^4 I[\ln(D_{e|d|c|IM}^p) \geq \ln(C_{l|e|d|c}^p)] \quad (25)$$

where $I[\cdot]$ is defined in Eq. (20); $D_{e|d|c|IM}^p$ is the demand of element e under the given IM, which can be acquired via Eq. (19); $C_{l|e|d|c}^p$ denotes the capacity for element e of component type c corresponding to damage state l , which is obtained via MCS while $C_{l|e|d|c}^p$ is assumed to follow a two-parameter lognormal distribution (median S_c and dispersion β_c) with the parameters listed in Table 1. The possible values (i.e., 0, 1, 2, 3, 4) of $DS_{e|d|c|IM}^p$ represent no damage, slight damage, moderate damage, extensive damage, and complete damage, respectively.

Four limit states of piers were defined according to moment-curvature curves, as shown in Fig. 2A. The limit states corresponding to slight damage and complete damage are determined by equivalent yield curvature φ_y and ultimate crushing curvature φ_u , respectively. The limit states for moderate damage and extensive damage are located at trisection points between φ_y and φ_u . The histograms of the frequency distribution of curvature ductility associated with the two limit states are plotted in Fig. 2B and C, considering material uncertainty of pier and axial seismic responses. Meanwhile, the kernel density

estimation (KDE) curve and the fitted probability density curve of lognormal distribution were also obtained. The good consistency of the two curves provides a basis for the lognormal distribution assumption.

The limit state definition of LRBs in longitudinal and transverse directions is exhibited in Fig. 3. The slight damage state of LRBs is determined with regard to the bearing critical sliding displacement (Δ_f), which can be acquired by the ratio of bearing friction force to elastic stiffness. The moderate damage state is defined once the bearing slides beyond the edge of the girder bottom, which corresponds to Δ_{t1} and Δ_{t2} . The complete damage state is characterized by bearing unseating displacement (Δ_{t3} and Δ_{l3}), while Δ_{t2} (Δ_{t3}) is defined as the midpoint of Δ_{t1} and Δ_{l3} (Δ_{t1} and Δ_{t3}). The bearing unseating is assumed to take place when the contact length between the LRB and girder is less than 7.5 cm [47].

After the determination of $DS_{e|d|c|IM}^p$, $L_{e|d|c|IM}^p$ can be written as:

$$L_{e|d|c|IM}^p = \sum_{l=1}^4 \sum_{q=1}^{n_{q|l|d|c}} \delta(l - DS_{e|d|c|IM}^p) \delta(q - A_{l|d|c|IM}^p) L_{q|l|d|c|IM}^p(X) \quad (26)$$

where $\delta(\cdot)$ is the Dirac delta function, $n_{q|l|d|c}$ is the total number of repair actions for damage state l , damage mode d and component type c , $A_{l|d|c|IM}^p$ is the sequence of the repair action selected probabilistically from the repair action database, and $L_{q|l|d|c|IM}^p(X)$ refers to the repair cost of the q -th repair action associated with various parameters. By combining Eqs. (22)–(26), the total repair costs for the given IM can be statistically expressed as:

$$E[L_T|IM] = \frac{1}{n_s} \sum_{p=1}^{n_s} \sum_{c=1}^{n_c} \sum_{d=1}^{n_{df|c}} \sum_{e=1}^{n_{el|df|c}} \sum_{l=1}^4 \sum_{q=1}^{n_{al|df|c}} \delta(l - DS_{e|d|c|IM}^p) \delta(q - A_{l|d|c|IM}^p) L_{q|l|d|c|IM}^p(X) \quad (27)$$

5. Cost-based optimization procedure

5.1. Design variables

Overpass bridges are generally designed as multi-girder bridges with a single span length less than 40 m. For economic concerns, LRBs are widely adopted to allow the movement of superstructure under both service- and earthquake-level loadings, while transverse shear keys work as excessive displacement stoppers. The rubber bearings are not bonded to the substructure or the girder for the convenience of construction. As a result, the maximum shear force transmitted to piers/abutments by LRBs is sliding friction force. During seismic design, bridge piers only need to retain elastic under maximum bearing shear force. So the seismic performance of overpass bridges mainly depends on the properties of LRBs, expansion joints, and restrainers.

In this study, CMEJs are adopted to restrain the relative displacement between abutment and girder. The gap size of CMEJs and the dimension of LRBs play important roles in the seismic response of skew overpass bridges. Unfortunately, there are no existing design specifications to determine the optimal parameters for these components of a specific bridge. As a result, the following three parameters are selected as design variables: the initial free movement between abutment and girder (Δ_f), contact area (A_B) and total rubber layer thickness (t_R) of the LRB. Bridges equipped with either CMEJs or MEJs are compared for seismic performance, and the variables for both types are optimized to facilitate the comparison.

5.2. Objective function

As mentioned in Section 1, the objective of the optimization is to minimize construction cost and expected repair cost related to bridge design variables, which can be expressed as:

$$\min F(X) = E[C_T|X] + E[L_T|X] \quad (28)$$

where $X = [x_1, x_2, \dots, x_m]$ is the set of design variables, $E[C_T|X]$ is the construction cost related to bridge design variables x . The construction cost of a modular expansion joint is set to \$934/m regardless of its gap size [26]. The construction cost of LRB is determined by its total number, the area (A_B) and the total rubber layer thickness (t_R) [48]. Accordingly, the considered construction cost is given by:

$$E[C_{\text{Bearing}}|X] = n_B \times (9623A_B + 7764t_B + 12) \quad (29)$$

To estimate the expected repair cost of a bridge while considering uncertainties in structure response, repair actions, cost of repair actions and seismic hazard, the expected repair cost is defined in Eq. (30) in accordance with the Pacific Earthquake Engineering Research (PEER) framework [49]:

$$E[L_T|X] = \int_0^\infty \int_0^\infty e^{-\eta\tau} E[L_T|IM, X] |d\nu(IM)| d\tau \quad (30)$$

where η is the discount rate per year (assumed to be 0.03 [50]), t is the design life of the bridge, $\nu(IM)$ is the annual rate of exceedance of given intensity measure, which is obtained from site-specific probabilistic seismic hazard analysis (PSHA). In this study, the hyperbolic model proposed by Bradley et al. [51] is adopted to approximate the seismic hazard curve:

$$\nu = \nu_{asy} \exp \left\{ \alpha \left[\frac{IM}{IM_{asy}} \right]^{-1} \right\} \quad (31)$$

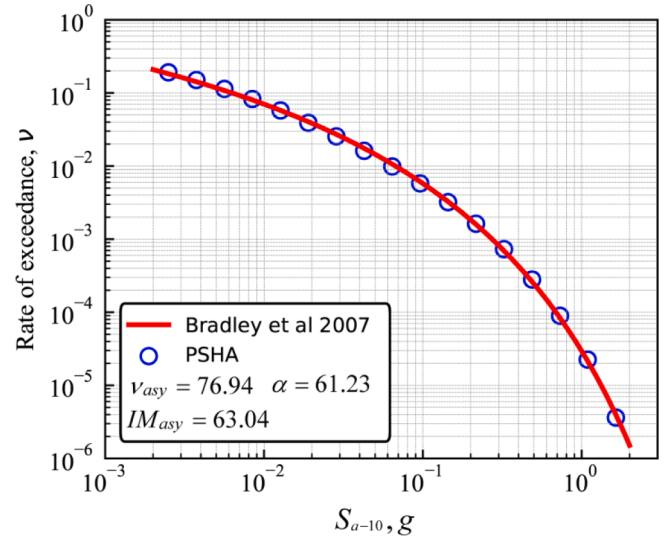


Fig. 4. Hazard curve fitted by Eq. (31).

where ν_{asy} , α and IM_{asy} are three unknown parameters, while ν_{asy} and IM_{asy} refer to the horizontal and vertical asymptotes of the hyperbolic curve. They can be determined using non-linear least-squares regression to minimize the logarithms of errors between PSHA data and the hyperbolic model, as shown in Fig. 4. To evaluate $E[L_T|x]$, numerical integration is performed over the full range of IM with respect to a given IM, and $|d\nu(IM)|$ is substituted by $|d\nu(IM)/dIM|dIM$ where $|d\nu(IM)/dIM|$ is the gradient of the seismic hazard curve. The range of spectral acceleration at 1.0 s (Sa10) greater than 0.01 g is considered to be sufficient since smaller Sa10s are not likely to cause notable structural damage. The contribution of Sa10s with return periods greater than 10^6 years ($\nu=10^{-6}$) is ignored when conducting probabilistic loss estimation [51].

5.3. Constraint

The feasible region of design parameters needs to be determined to satisfy the requirement of design specification. To ensure the normal functions of bearings under service-level loading, sufficient compressive capacity and adequate allowable shear deformation must be guaranteed, the area and the total thickness of rubber layers should be constrained as follows:

$$A_B \geq \frac{R_{ck}}{\sigma_B} \quad (32)$$

$$t_R \geq 2\Delta_t \quad (33)$$

where R_{ck} is the design value of bearing reaction force, σ_B is the allowable average compressive stress of LRBs (defined based on specification [52]), Δ_t refers to the deformation of LRB due to temperature, shrinkage, and creep. Sliding of bearing is prohibited under service-level loading, and friction is given as:

$$\mu N_B \geq 1.4 G_B A_B \frac{\Delta_t}{t_R} \quad (34)$$

where G_B and A_B is the shear modulus and the area of the LRB, μ is the friction coefficient between rubber and concrete, N_B refers to the reaction force of the bearing under gravity load. Moreover, considering the compression stability of LRB, Eq. (35) and Eq. (36) should be satisfied for circular and rectangular LRB, respectively:

$$\frac{d_B}{10} \leq t_R \leq \frac{d_B}{5} \quad (35)$$

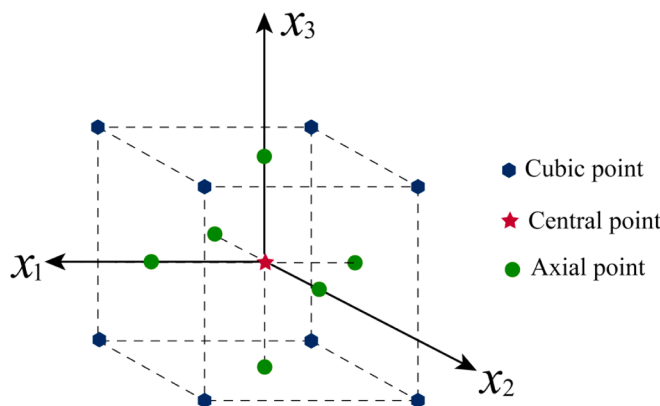


Fig. 5. sampling points of the three-factorial CCD.

$$\frac{l_B}{10} \leq l_R \leq \frac{l_B}{5} \quad (36)$$

where \$d_B\$ is the diameter of circular LRBs, \$l_B\$ is the shorter side length of rectangular LRB.

For the expansion joints, the minimum free movement displacement is given by:

$$\Delta_J \geq 2\Delta, \quad (37)$$

5.4. Response surface method

For the procedure of probabilistic seismic loss assessment (PSLA), it is suggested that 80 or more times of nonlinear time history analyses (NTHAs) are necessary to ensure the reliability of the PSDM [53]. Hundreds of PSLAs should be considered for conventional iterative-based optimization algorithms, which leads to an unacceptable cost of computation. To resolve the issue, the response surface method (RSM) is introduced to balance efficiency and accuracy by fitting the real response surface with a polynomial function in the interested region of design parameters. The RSM includes two steps: (1) experimental design and (2) response surface fitting. In this study, the central composite design (CCD) technique is adopted to select sampling points [54]. These

sample points consist of cubic points, central points, and axial points, which are typically coded as \$\pm 1\$, \$0\$, and \$\alpha\$ (\$\alpha\$ refers to the distance from the axial point to the central point). For a three-factorial design, eight cubic points, eight central points, and six axial points are employed, as shown in Fig. 5 (\$\alpha=1\$). The reliability of such a design has been proved by Towashiraporn [55]. Certain sampling points may not be consistent with Eqs. (32)–(37), but they are still necessary for establishing the response surface. After the PSLA of each sampling point, the expected repair cost under each parameter condition is acquired, and the response function can be expressed in the form of second-order polynomial function:

$$F(X) = u_0 + \sum_{i=1}^m u_{ii}x_i + \sum_{i=1}^m u_{ii}x_i^2 + \sum_{i=1}^{m-1} \sum_{j>i}^m u_{ij}x_i^2 + \varepsilon \quad (38)$$

where \$X = [x_1, x_2, \dots, x_m]\$ is the set of design parameters \$u_0, u_{ii}\$ and \$u_{ij}\$ are coefficients to be determined by the least squares method, \$\varepsilon\$ refers to the residual error.

Finally, to obtain the optimal parameter combination in the feasible region, the particle swarm optimization (PSO) approach is implemented while the constraints are considered by means of penalty functions. PSO is a kind of heuristic algorithm that can solve the minimization problem of continuous nonlinear functions efficiently [56]. Summarizing the components of the optimization procedure, the cost-based optimization procedure is given in Fig. 6. The PSHA for specific bridges should be done by the seismological bureau in China.

6. Bridge model

6.1. Description and numerical simulation

The prototype bridge is a typical skew continuous overpass with a total length of 90 (30 \$\times\$ 3) m, a width of 12.8 m, and a skew angle of 30°. The deck consists of four small box girders (2.4 m in width and 1.6 m in depth). Four diaphragms are placed along each span of the bridge. The superstructure is supported by cap beams (1.8 m in width and 1.6 m in depth). The circular piers have a diameter of 1.6 m and a height of 15 m. The reinforcement ratio and the volumetric stirrup to concrete ratio are 1 % and 0.6 %, respectively. Each pier is supported by a pile with a diameter of 1.8 m and a depth of 25 m. The soil profile consists of a

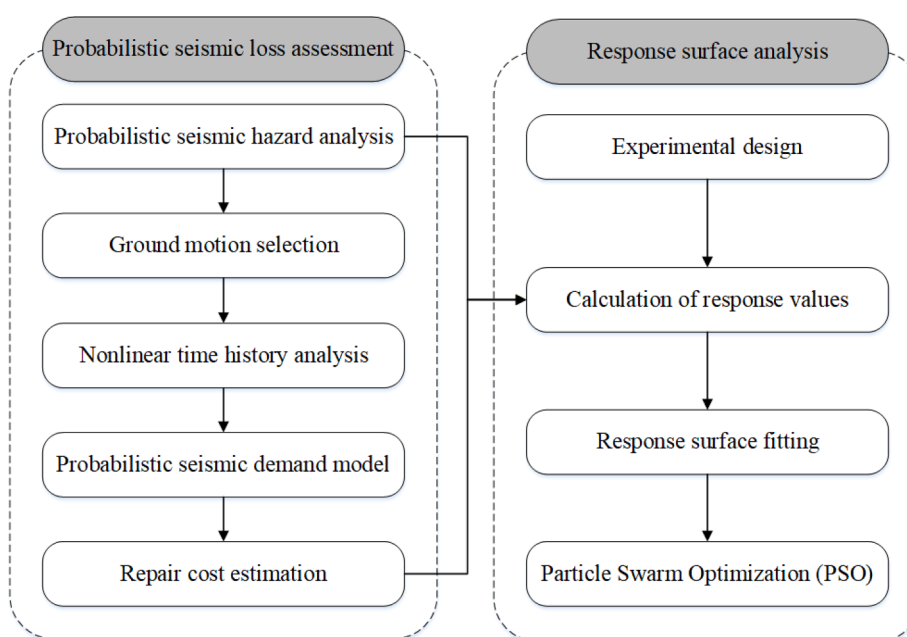


Fig. 6. Cost-based optimization procedure.

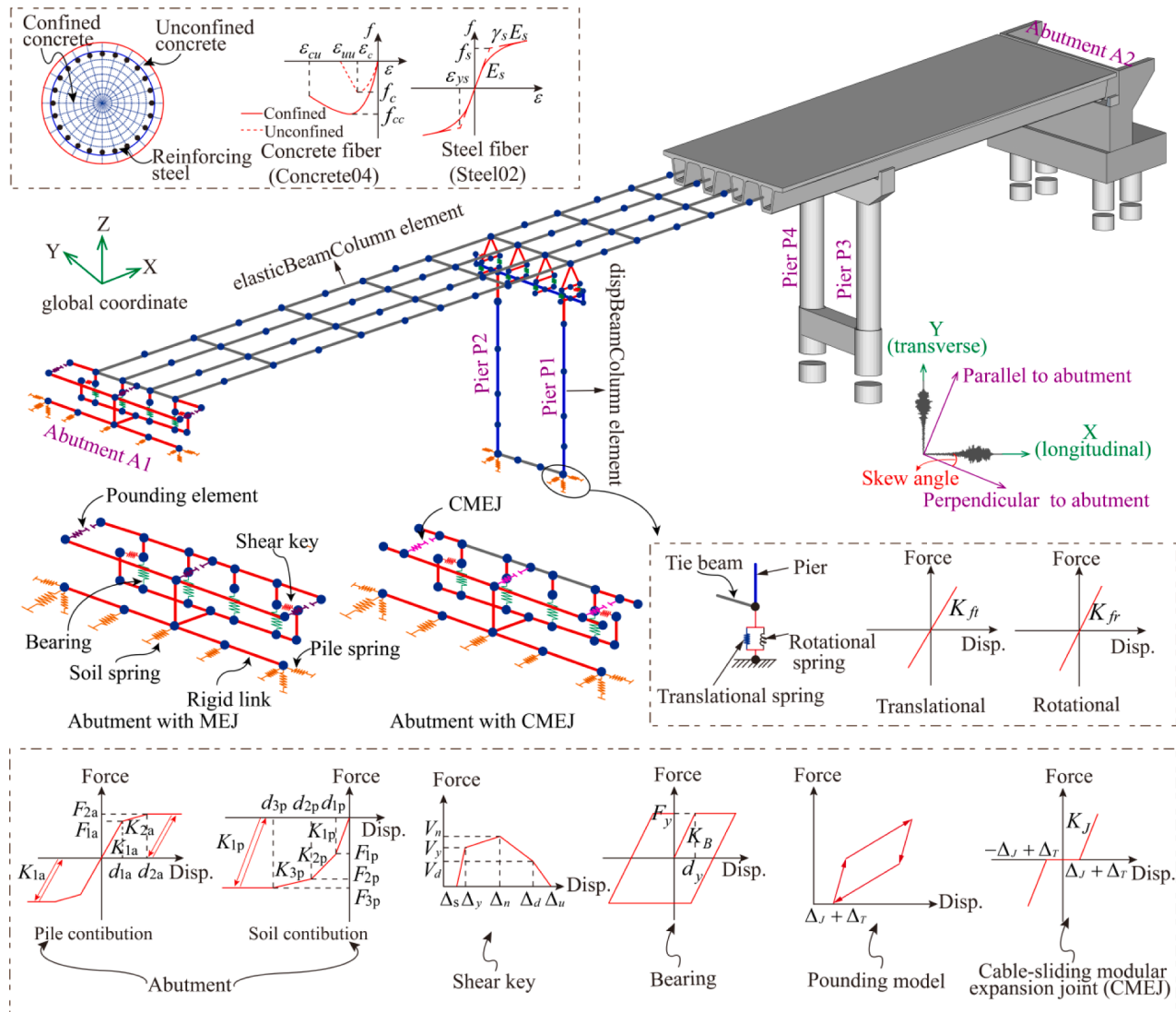


Fig. 7. Generic model used for nonlinear history analysis.

debris layer topped by stiff clay followed by soft clay with a sickness of 5.5 m, 13.4 m, and 6.1 m. The bridge ends are supported by abutments (13 m in width and 6 m in depth). Each pier is supported on four 1.5 m piles with a depth of 20 m. The abutment profile consists of a 10.2 m stiff clay layer and a 9.8 m soft clay layer. Circular laminated rubber bearings are used in this case. The deck is constructed using C50 (nominal compressive strength $f_{ck} = 32.4$ MPa) concrete; the piers are with C40 ($f_{ck} = 26.8$ MPa) concrete and HRB400 (nominal yield strength $f_{sk} = 400$ MPa) steel rebars, while C30 ($f_{ck} = 20.1$ MPa) concrete is adopted for the foundations and abutments. The ultimate tensile strength of the CMEJ is designed as 1.5 times the total dead load reaction of bearings on an abutment [57]. Such constraint enables the CMEJ to prevent the unseating side of the girder from falling in case of an extreme earthquake.

The Finite element model is established in OpenSees. The constitutive relationships and the simulation details of the numerical model are exhibited in Fig. 7. It is worth noticing that the longitudinal/traffic direction is considered along the global X-axis while the transverse direction is in the orientation of the global Y-axis. Since the deck usually remains elastic under earthquakes, it is simulated using elastic beam-column elements with mass lumped on deck nodes. Piers are simulated using displacement-based beam-column elements with fiber section that consists of reinforcement bar, cover concrete, and core

concrete. The stress-strain relationship of rebar was modeled using “Steel02” material, and the nonlinear behavior of cover and core concrete was defined according to Mander et al. [58] and simulated by “Concrete04” material in OpenSees. The shear span-to-depth ratio of the piers is large enough (1:0.11) to ensure that bending failure occurs prior to shear failure. The LRBs were modeled by zero-length elements. Horizontal stiffness (K_B) and yield force (F_y) of the bearing are calculated from Eq. (39).

$$K_B = \frac{G_B A_B}{t_R}, F_y = \mu N_B \quad (39)$$

The soil structure interplay (SSI) was considered with three translational and three rotational linear springs, and their stiffness was derived in accordance with reference [59]. Abutments were simulated by pile and soil springs. To ensure the direction of backfill passive pressure was perpendicular to abutment backwall, abutment springs were rotated in accordance with the abutment skew. The soil model developed by Nielson [60] was modified by changing the stiffness and yield strength under the assumption that the stiffness and strength of soil springs increase linearly as a function of distance from the obtuse corner. Following the study of Kaviani et al. [61], the stiffness/strength variation coefficient κ_s for a given skew angle β is defined as $0.3 * \tan(\beta) / \tan(60^\circ)$, which means the stiffness/strength of acute spring

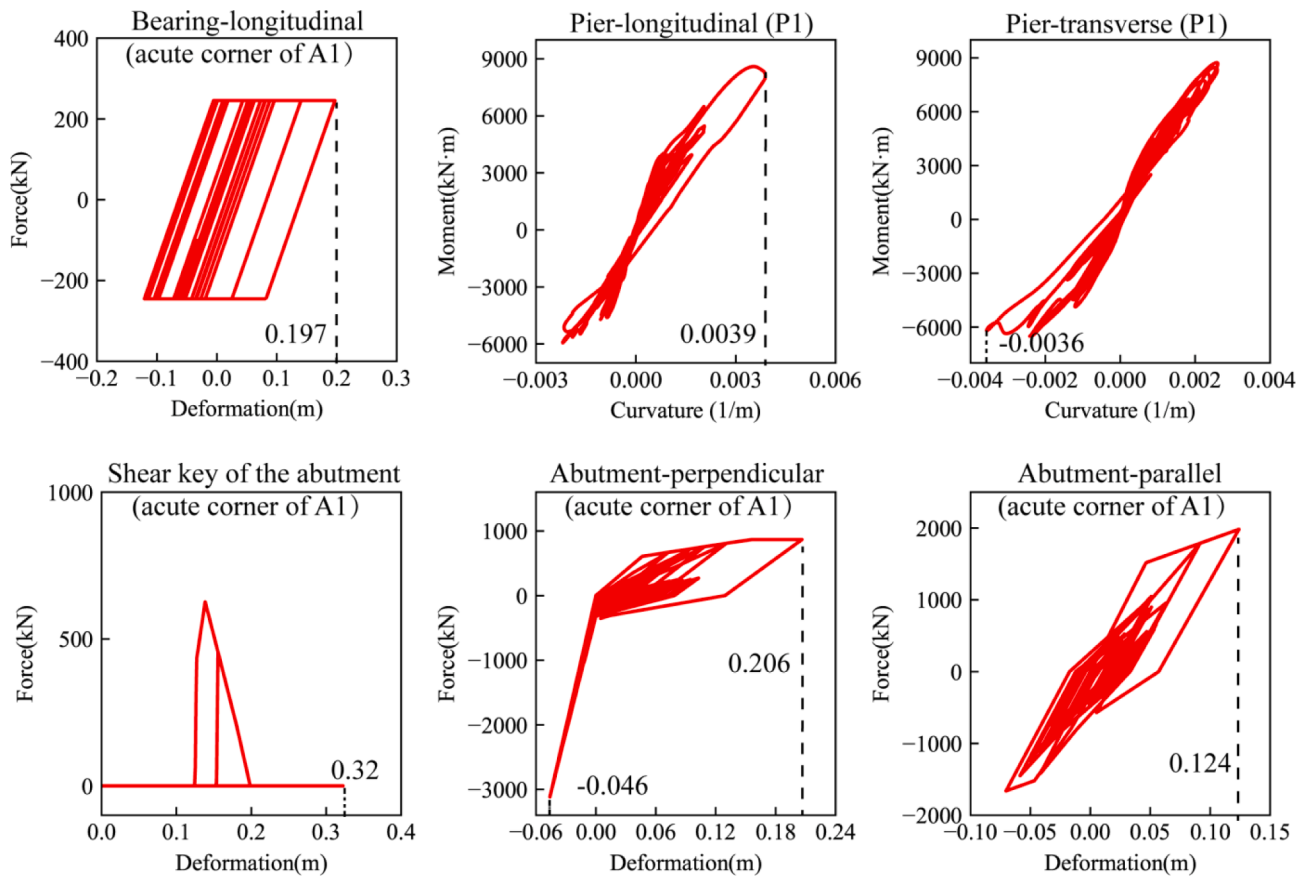


Fig. 8. Hysteretic curves of bridge components.

is $(1 + \kappa_s)$ times the original model. Active stiffness of abutments is solely provided by piles. The symmetric trilinear model was adopted to capture the nonlinear behavior of piles [60]. The effects of shear keys were reproduced by zero-length nonlinear elements with the constitutive relationships proposed by Xu et al. [62]. The gap size between shear keys and the girder was determined as 2.5 times the total rubber layer thickness of LRBs.

When MEJs were adopted, the pounding effect between abutments and girder should be considered. The pounding effect was simulated using a zero-length element with the nonlinear model proposed by Muthukumar [63], which is a bilinear model with a gap. The initial stiffness and second stiffness are 179 kN/mm and 62 kN/mm, respectively. The maximum deformation is assumed to be 25.4 mm and the yield deformation is 10 % of the maximum deformation. If CMEJs were used, truss elements with the constitutive model shown in Fig. 1C were adopted to model CMEJs. The stiffness of CMEJs is 131 kN/mm. The “MinMax” material was used to specify an upper bound of cable strains, which can detect axial tensile failure of the cables. The ultimate stress of cables is considered as 1960 MPa. The actual gap size of MEJs and CMEJs is the initial free movement between abutment and girder Δ_f plus the temperature-induced abutment-deck deformation Δ_T . Rayleigh damping was adopted for the first and tenth vibration modes so that the damping within the interested periods would distribute around 5 %.

To observe the vibration characteristic of the bridge equipped with the MEJ, the 1994 Northridge earthquake recorder (Recorder sequence number is 1087, the peak ground accelerations of two horizontal components are 0.99 g and 1.78 g.) obtained from the PEER NGA-West2 database was adopted as an example input ground motion and the hysteretic curves of individual components were exhibited in Fig. 8.

6.2. Uncertainty treatment

In the probabilistic-based seismic loss estimation, it is necessary to consider the uncertainty of modeling-related uncertain parameters since the EDP may depend on the coupled contribution from the uncertainty of modeling-related parameters and ground motion [64]. According to previous studies, 15 critical modeling-related uncertain parameters were considered, which mainly fall into three aspects: material-related parameters, structural-related parameters, and boundary condition-related parameters. The probability distribution, mean value, coefficient of variation (CV), or standard deviation (SD) of each considered modeling-related uncertain parameter are listed in Table 2. The correlation coefficients of different pairs of modeling-related uncertain parameters are assumed as follows: $\rho = 0.8$ for ϵ_c and ϵ_{uu} , $\rho = 0$ for all other pairs of parameters. Nataf transformation [65] and Latin Hypercube sampling (LHS) technique are adopted to establish one hundred cases of each modeling-related uncertain parameter considering the correction between parameters. As a result, one hundred bridge models, paired with one hundred selected ground motion records (described in Section 6.3), are used in nonlinear time history analyses.

6.3. Ground motions

The accuracy and reliability of PSDM greatly depend on the characteristics of ground motions. The algorithm proposed by Baker and Lee [73] can select a set of ground motions from a database while matching a target mean and variance of logarithmic spectral acceleration values generated by the ground motion prediction model (GMPM). As a result, the uncertainty of ground motions is considered during the PSHA. Near-fault and far-field ground motions are not distinguished during ground motion selection. Based on site conditions, the average shear wave velocity in the top 30 m (V_{30}) is 215 m/s, and the median and the

Table 2
Uncertainty parameters of bridges and their probability distribution.

Name	Description	Units	Distribution	Distribution parameters
Material-related parameters				
f_c	Cover concrete compressive strength [66]	MPa	Normal	Mean = 40, SD = 4.8
ϵ_c	Cover concrete strain at peak strength [67]		Lognormal	Mean = 0.002, CV = 0.2
ϵ_{uu}	Cover concrete strain at crushing strength [67]		Lognormal	Mean = 0.006, CV = 0.2
λ_w	concrete weight coefficient [60]		Uniform	Lower = 0.9, Upper = 1.1
f_s	Rebar yield strength [68]	MPa	Normal	Mean = 448, SD = 35.84
E_s	Young's modulus of steel rebar [67]	GPa	Lognormal	Mean = 201, CV = 0.033
γ_s	Rebar post-yield to initial stiffness ratio [67]		Lognormal	Mean = 0.005, CV = 0.2
G_B	Bearing shear modulus [69]	MPa	Uniform	Lower = 0.7, Upper = 1.1
Structural-related parameters				
μ	Coefficient of friction of bearing pad [70]		Normal	Mean = 0.3, SD = 0.1
ξ	Damping ratio [64]		Normal	Mean = 0.05, SD = 0.01
Δ_T	Temperature-induced abutment-deck gap [71]	mm	Normal	Mean = 0, SD = 18
Boundary condition-related parameters				
$K_{passive}$	Passive stiffness of abutments [72]	kN/mm/m	Normal	Mean = 20.2, SD = 3.02
K_{active}	Active stiffness of abutments [72]	kN/mm/m	Normal	Mean = 7, SD = 1.05
K_{ft}	Translational stiffness of Piles [70]	kN/mm	Lognormal	Mean = as calculated by specifications [59], CV = 0.44
K_{fr}	Transverse rotational stiffness of Piles [70]	kN/mm	Lognormal	Mean = as calculated by specifications [59], CV = 0.28

logarithmic standard deviation of the log-space response spectra were predicted for a magnitude of 7 and a rupture distance of 20 km [74]. One hundred ground motions are selected from the NGA-West2 database with the following selection criteria: (a) moment magnitude (M) ranges from 5 to 8; (b) the closest distance to the surface projection of fault rupture (R_{jb}) is less than 120 km; (c) V_{30} varies from 150 to 260 m/s. Fig. 9A shows the acceleration response spectra (5 % damping) for each

ground motion, together with the mean spectra and 95 % confidence interval. Statistics of magnitude and rupture distance are shown in Fig. 9B. In this study, the seismic input direction for the bridge model is only limited to longitudinal and transverse directions.

7. Probabilistic seismic demand analysis

7.1. Optimal IM for the prototype bridge

To establish a proper PSDM, EDPs and the IM should be selected first. Earthquake-induced damage in abutments, bearings, and columns of continuous bridges has been observed in past earthquakes [75]. In this regard, passive abutment displacement (δ_p), active abutment displacement (δ_a), bearing displacement (δ_{bl} and δ_{br}), and curvature ductility of the pier (μ_c) are selected as EDPs. Besides, a suitable IM helps reduce the level of variability and improve the reliability of the PSDM. As given in Table 3, ten commonly used IMs with determined seismic hazard curves are chosen [76]. Structure-dependent IMs (i.e., spectral acceleration at the structure vibration periods) exhibit lower hazard computability than structure-independent IMs and are not considered in this study.

The optimal IM was selected based on the criteria of efficiency, practicality, proficiency, correlation, and sufficiency [39,40]. Better efficiency is represented by a lower standard deviation of regression residuals (β_D, β'_D). Better practicality is indicated by a higher slope (b, b') which refers to the dependency of structural demand upon given IM. The composite effectiveness is measured by the proficiency parameter ζ defined as:

$$\zeta = \beta_D/b \text{ or } \zeta = \beta'_D/b' \quad (40)$$

Table 3
considered intensity measures in this study.

IM	Description	Definition
PGA	Peak ground acc.	$\max\{ a(t) , a(t)\}$, $a(t)$ is the acc. time history
PGV	Peak ground vel.	$\max\{ v(t) , v(t)\}$, $v(t)$ is the vel. time history
PGD	Peak ground disp.	$\max\{ u(t) , u(t)\}$, $u(t)$ is the vel. time history
AI	Arias Intensity	$\frac{\pi}{2g} \int_0^{tot} a^2(t) dt$, tot is the total duration
A_{rms}	Root-mean-square of acc.	$\sqrt{1/t_d \int_{t_1}^{t_2} a^2(t) dt}$, $t_d = t_2 - t_1$, $t_2 = t(5\%AI)$, $t_1 = t(95\%AI)$
ASI	Acc. spectrum intensity	$\int_{0.1}^{0.5} S_a(\xi = 0.05, T) dT$
VSI	Vel. spectrum intensity	$\int_{0.1}^{2.5} S_v(\xi = 0.05, T) dT$
CAV	Cumulative absolute vel.	$\int_0^{tot} a(t) dt$
S_{a-02}	Spectral acc. at 0.2 s	$S_a(\xi = 0.05, T = 0.2s)$
S_{a-10}	Spectral acc. at 1.0 s	$S_a(\xi = 0.05, T = 1.0s)$

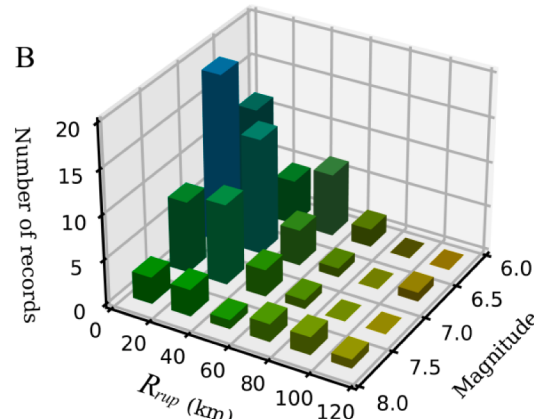
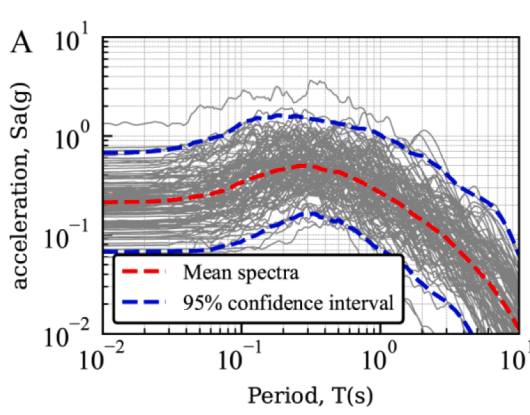


Fig. 9. Properties of selected ground motion suite: (A) acceleration response spectra (5 % damping), (B) M-R distribution.

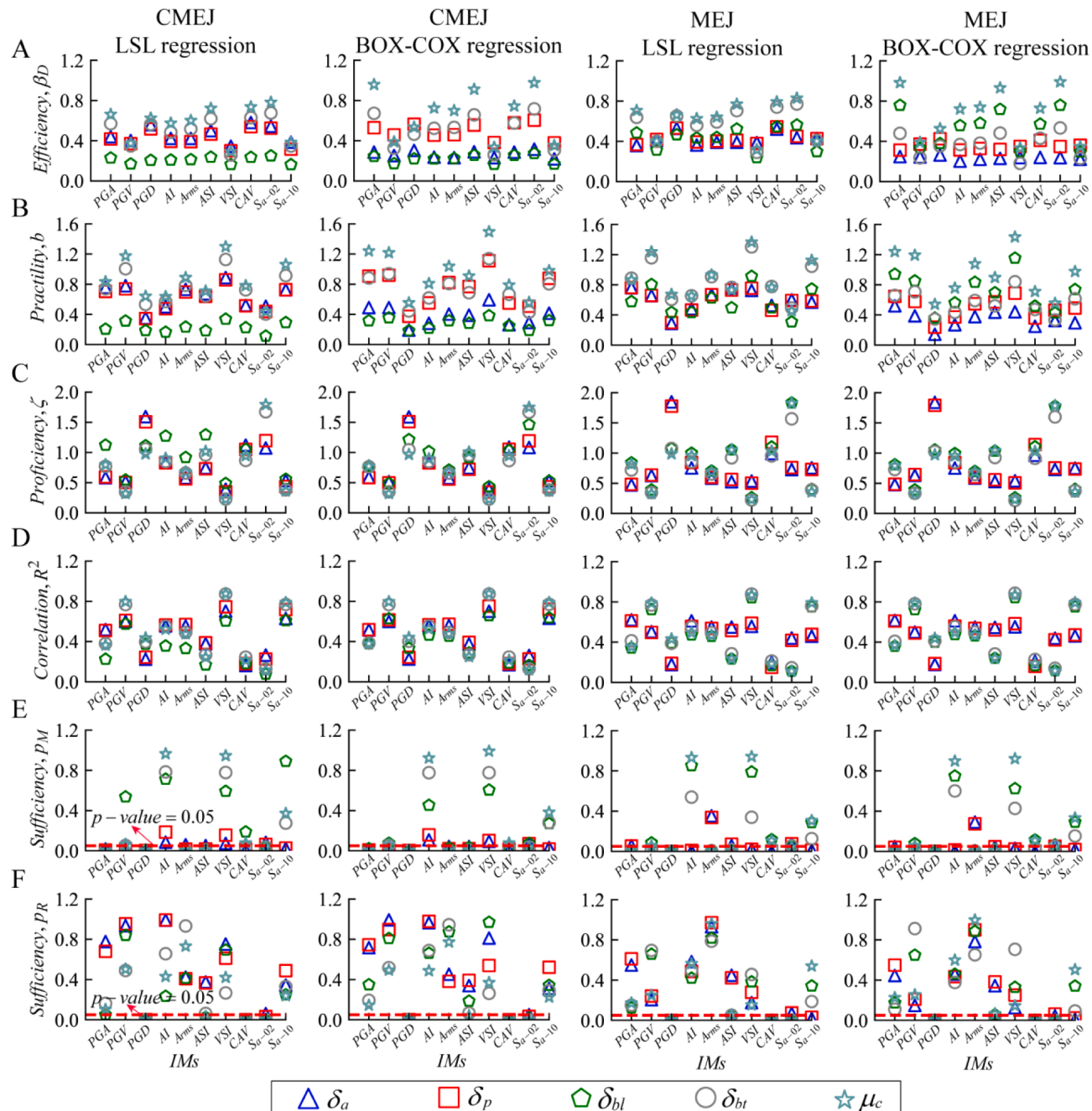


Fig. 10. Comparisons of studied IMs in terms of (A) efficiency, (B) practicality, (C) proficiency, (D) correlation, (E) sufficiency with regard to p_M , (F) sufficiency with regard to p_R .

where a smaller ζ implies a more proficient IM.

The determination coefficient (R^2) is used to indicate the degree of regression model fitting. It is the square of the correction coefficient, which is between 0 and 1. A higher R^2 value indicates a better correlation. A sufficient IM is conditionally statistically independent from ground motion characteristics, such as magnitude (M) and source-to-site distance (R). The sufficiency of an IM is quantified by regression analysis on the residuals from PSDM. The p -value for the linear regression of residuals on M or R (p_M , p_R) is used to evaluate the sufficiency, and p -values smaller than 0.05 usually refer to an insufficient IM.

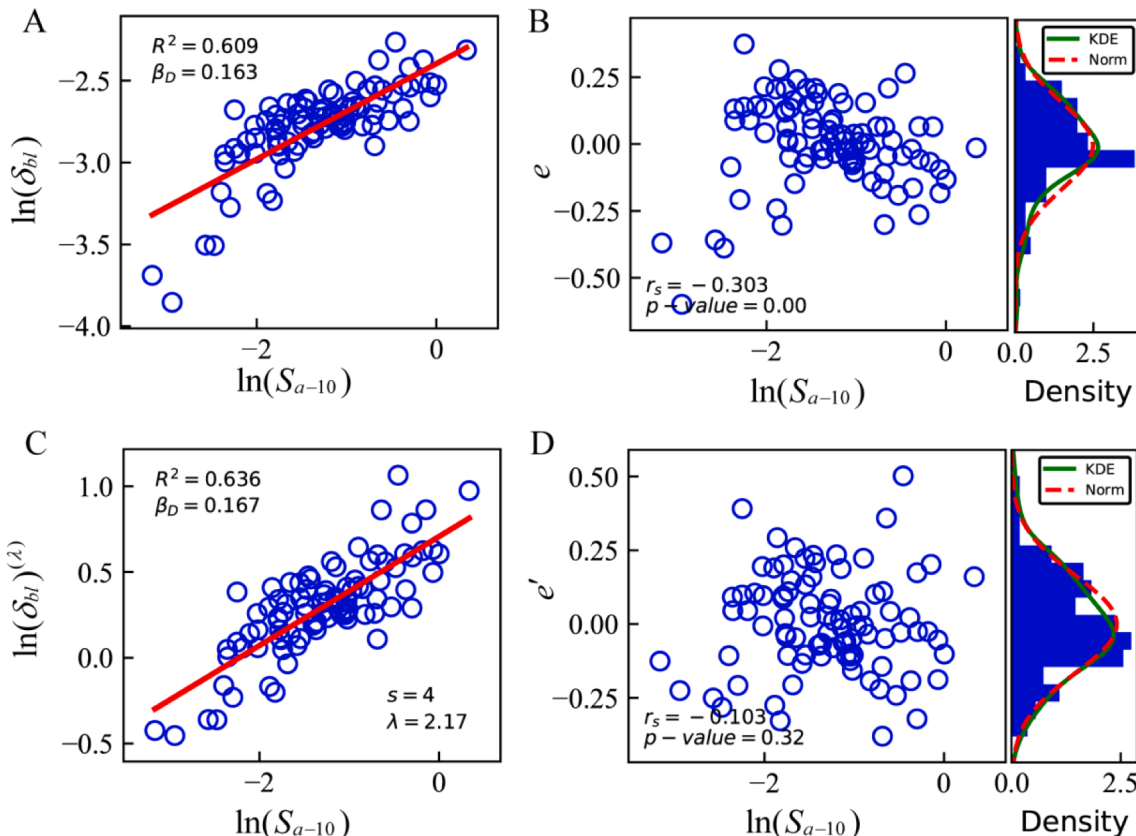
Displacement of abutment A1 (δ_p and δ_a), displacement of the bearing on the acute corner of abutment A1 (δ_{bl} and δ_{bt}), and curvature ductility at the bottom of pier P1 are selected as the representative EDPs. Without loss of generality, design variables of Δ_J , A_B , and t_R are taken as

0.1 m, 0.32 m², and 0.1 m, respectively. Comparison of the IM candidates is illustrated in Fig. 10 with various regression models and different expansion joints. As shown in Fig. 10A-D, the difference in regression models imposes a significant impact on the efficiency and practicality of IMs, but the rankings of proficiency and correlation for the two regression models are at the same level. Therefore, it is suggested that proficiency can be served as the primary factor, while efficiency and practicality may be deemed as secondary factors, which is consistent with previous studies [38]. On the other hand, there is a high consistency between the rankings of proficiency and correlation, which implies that the R^2 is another index for proficiency. In terms of proficiency, PGV, VSI, and S_{a-10} show better performance, while acceleration-related IMs and displacement-related IMs are of lower performance. Fig. 10E and F show the comparative assessment of

Table 4

Results of LSL regression and BOX-COX regression.

EDP	LSL regression			BOX-COX regression				
	R^2	r_s	p-value	s	λ	R^2	r_s	p-value
δ_p	0.718	-0.087	0.41	6	1.26	0.721	-0.028	0.79
δ_a	0.629	0.000	1.00	6	0.47	0.632	-0.101	0.33
δ_{bl}	0.609	-0.303	0.00	4	2.17	0.636	-0.103	0.32
δ_{bt}	0.769	0.068	0.52	5	0.87	0.770	0.036	0.73
μ_c	0.788	0.074	0.48	4	0.93	0.788	0.048	0.65

**Fig. 11.** Comparison of LSL regression and BOX-COX regression with respect to δ_{bt} : (A) PSDM based on LSL regression, (B) residual errors of LSL regression, (C) PSDM based on BOX-COX regression, (D) residual errors of BOX-COX regression.

sufficiency with respect to p_M and p_R . It is found that most IMs are sufficient with respect to source-to-site distance (R), while almost all the IM candidates are insufficient with respect to magnitude (M). In addition, hazard information of S_{a-10} is readily available across the site-specific probabilistic seismic hazard analysis report. In general, AI , VSI and S_{a-10} perform better in terms of sufficiency. Considering all the selected criteria, VSI and S_{a-10} are deemed as the most suitable IMs for the prototype bridge, and S_{a-10} is thus selected as the optimal IM.

7.2. Probabilistic seismic demand models

PSDMs for five EDPs are developed based on least squares linear (LSL) regression and BOX-COX regression. To evaluate the normality of residual error e , histograms of the frequency distribution of e are plotted. Meanwhile, the KDE curve and the fitting normal distribution curve are obtained. The normality assumption requires consistency between the two curves. The determination coefficient (R^2) is adopted to quantitatively evaluate the linearity of the regression model. The rank correlation coefficient method is used to identify heteroscedasticity [77]. Sorting x and $|e|$, respectively, are required when calculating (r_s):

$$r_s = 1 - \frac{6}{n(n^2 - 1)} \sum_{i=1}^n d_i^2 \quad (41)$$

where d_i is the ranked difference between x_i and $|e_i|$. The p -value is obtained by the significance test of r_s , and heteroscedasticity is tested with a significance level of 0.05 [78].

The parameters of LSL regression and BOX-COX regression are listed in Table 4. Significant heteroscedasticity exists in LSL regression models when δ_{bt} is taken as EDP. Heteroscedasticity is eliminated when BOX-COX regression is adopted. For the EDP of δ_{bt} , the R^2 of BOX-COX regression is increased by 4.4 %, compared with LSL regression. It implies that there is a nonlinear correlation between the independent variable and the response variable when the linearity of the BOX-COX regression is increased. Three basic assumptions of the cloud method are satisfied when δ_p , δ_a , δ_{bt} and μ_c are adopted as the EDP, which indicates that the cloud method is feasible in most cases.

PSDMs based on LSL regression and BOX-COX regression with respect to δ_{bt} are plotted as shown in Fig. 11. Meanwhile, residual graphs are acquired by subtracting prediction values from actual values, and the KDE of residual errors and the fitted normal distribution (Norm) are

Table 5
Sampling points of the CCD.

cases	A_B (m^2)	t_R (m)	Δ_J (m)	$F(X)$ for MEJ (\$)	$F(X)$ for CMEJ (\$)
1	0.32	0.05	0.10	1,554,774	1,590,092
2	0.32	0.10	0.10	1,453,141	1,360,158
3	0.32	0.10	0.05	1,419,430	1,277,416
4	0.32	0.10	0.10	1,456,152	1,366,698
5	0.32	0.10	0.10	1,453,172	1,361,607
6	0.32	0.15	0.10	1,411,747	1,285,833
7	0.32	0.10	0.10	1,451,003	1,357,098
8	0.18	0.05	0.05	1,356,128	1,242,902
9	0.45	0.10	0.10	1,636,032	1,568,355
10	0.18	0.05	0.15	1,378,568	1,411,479
11	0.45	0.15	0.05	1,516,275	1,319,741
12	0.18	0.15	0.15	1,330,435	1,238,061
13	0.45	0.05	0.05	1,704,907	1,634,193
14	0.32	0.10	0.10	1,452,009	1,355,447
15	0.32	0.10	0.15	1,461,837	1,419,304
16	0.18	0.15	0.05	1,298,985	1,234,299
17	0.18	0.10	0.10	1,322,343	1,227,325
18	0.45	0.15	0.15	1,561,916	1,475,707
19	0.32	0.10	0.10	1,460,302	1,350,539
20	0.45	0.05	0.15	1,717,885	1,735,208

obtained. Fig. 11 also shows the variation of the variance of LSL regression residuals with regard to different ground motion intensity, which indicates that the variance of LSL regression residuals depends on ground motion intensity. In the case of weak ground motions, the LSL regression residuals are more significant compared to the case of strong ground motions. After the BOX-COX regression is applied, the variance of residuals can be considered constant, and residuals obey stable normal distribution.

8. Optimization results and discussion

Based on practical engineering applications, the upper bounds of the

design parameters (Δ_J , A_B and t_R) are determined as 0.15 m, 0.45 m^2 , and 0.15 m, respectively. Twenty sampling points are generated according to CCD. The objective functions with respect to MEJ and CMEJ are obtained based on Section 5.2. The details of each case are shown in Table 5. The ratio of objective function values corresponding to the MEJ and the CMEJ depends on the design parameters, and therefore it is necessary to find the optimal parameters for the CMEJ and the MEJ before estimating the seismic mitigation efficiency.

The regression coefficients of fitted quadratic polynomial response surfaces are listed in Table 6 after rounding off insignificant terms (p -value > 0.1). Determination coefficients (R^2) and adjusted determination coefficients (R_{adj}^2) are greater than 0.9, indicating that the response surface models are reliable. The response surfaces are plotted as a function of the design parameters (A_B and t_R) in Fig. 12, along with nonlinear boundaries corresponding to the four constraint functions. The optimum design parameters are determined by the PSO approach, while the constraints are considered by means of penalty functions. The optimal parameters (Δ_J , A_B and t_R) are determined as 0.18 m, 0.09 m^2 and 0.05 m for both bridges with CMEJs and MEJs.

Fig. 13A compares the expected repair cost at a given level of ground motion intensity ($E[L_T|IM,X]$) with the optimal parameters. The expected repair cost can be further separated into the contribution of different types of bridge components (abutments, bearings, and piers):

$$E[L_c|X] = \int_0^{\infty} \int_0^{\infty} e^{-\eta\tau} E[L_c|IM,X] d\nu(IM) d\tau \quad (42)$$

where $E[L_c|IM,X]$ is the expected repair cost of a type of component conditioned on a specific intensity measure and design parameters. It can be evaluated by modifying Eq. (22):

$$E[L_c|IM,X] = \frac{1}{n_s} \sum_{p=1}^{n_s} L_{c|IM,X}^p \quad (43)$$

Table 6
Quadratic polynomial regression results.

Cases	Intercept (10^6)	Coefficient (10^6)		Δ_J	$A_B t_R$	$A_B \Delta_J$	$t_R \Delta_J$	A_B^2	t_R^2	Δ_J^2	R^2	R_{adj}^2
0°-MEJ	1.24	0.58	-0.72	-0.05	-4.64	/	7.04	1.63	/	/	0.98	0.97
0°-CMEJ	1.12	1.82	-4.21	1.13	-7.70	/	/	22.57	/	/	0.96	0.94
15°-MEJ	1.16	0.83	-2.42	2.94	-4.86	/	/	1.21	12.89	-11.67	0.99	0.99
15°-CMEJ	1.09	1.92	-3.84	1.14	-8.85	/	/	22.31	/	/	0.96	0.95
30°-MEJ	1.21	0.80	-1.78	1.73	-4.43	/	/	1.14	9.93	-7.12	0.99	0.99
30°-CMEJ	1.12	1.75	-4.02	1.14	-7.26	/	/	20.94	/	/	0.95	0.93
45°-MEJ	1.27	0.21	0.09	0.33	-3.38	/	/	1.94	/	/	0.99	0.99
45°-CMEJ	1.12	1.82	-4.11	1.04	-7.95	/	/	22.56	/	/	0.94	0.92
60°-MEJ	1.34	0.30	-2.25	1.13	-2.54	2.47	/	1.66	9.36	-6.67	0.99	0.99
60°-CMEJ	1.12	1.81	-3.97	0.99	-7.97	/	/	21.73	/	/	0.95	0.93

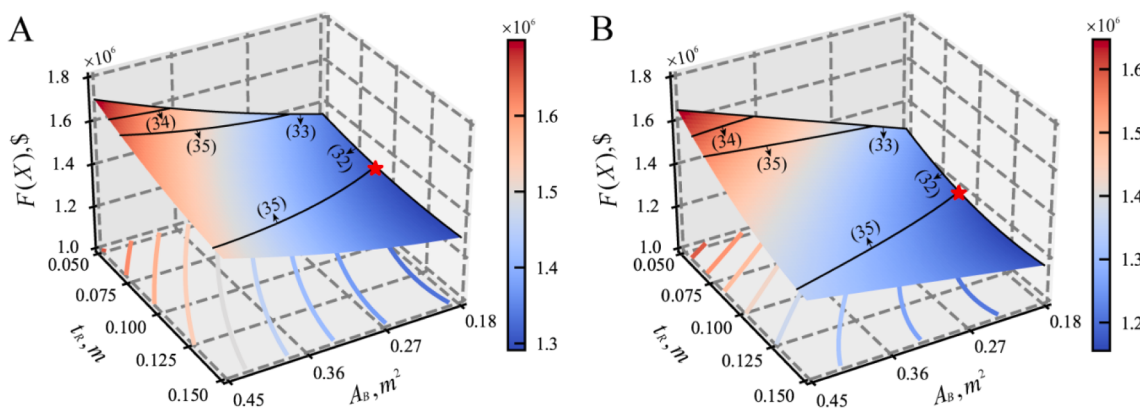


Fig. 12. Graphical representation of the response surface: (A) MEJ with a Δ_J of 0.05 m, (B) CMEJ with a Δ_J of 0.05 m.

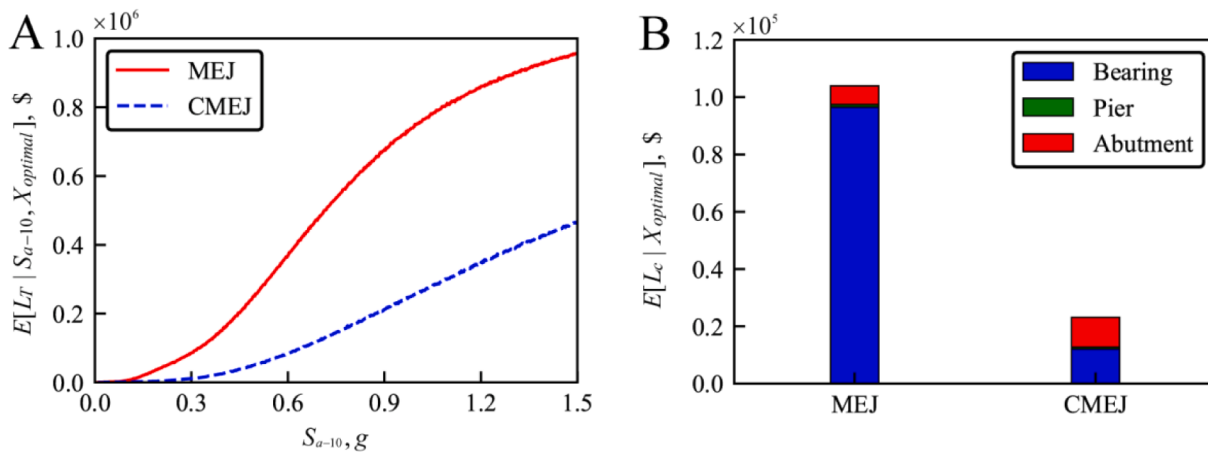


Fig. 13. Comparison of the expected repair cost with respect to the MEJ and the CMEJ: (A) means values of repair cost as a function of the S_{a-10} , (B) separated expected repair cost.

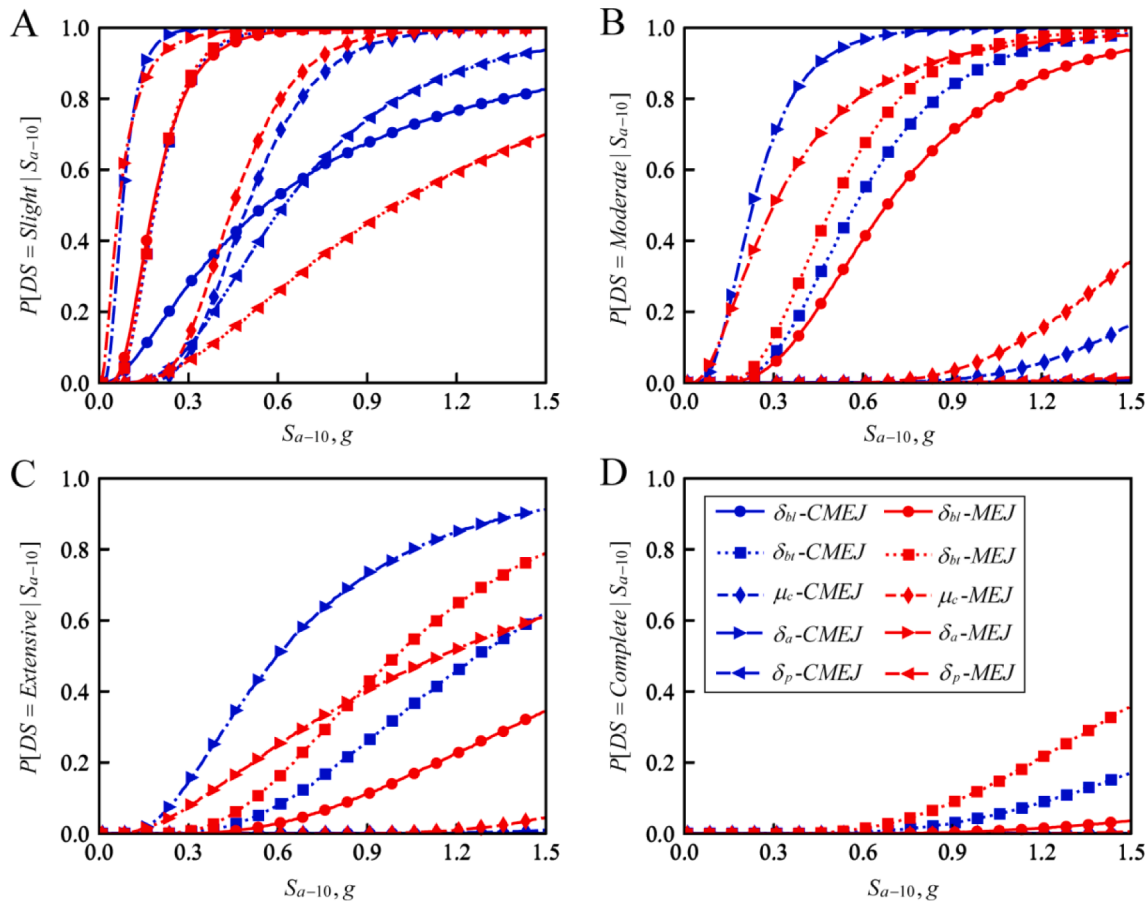


Fig. 14. Fragility curves with respect to the MEJ and the CMEJ: (A) slight damage, (B) moderate damage, (C) extensive damage, (D) complete damage.

Fig. 13B presents the individual expected repair cost for the case study bridge based on its contribution from different component types. Repair cost estimation of the bearings dominates the expected repair cost of the bridge with MEJs. Compared with MEJ, the expected repair cost of bearings with CMEJs decreases by 87.5 %, while that of abutments increases by 58.2 %. This is consistent with the fragility analysis results of Section 3.4 (Fig. 14). Bearings of the bridge with CMEJs retain lower damage probability than the ones with MEJs. However, CMEJ also increases the damage probability of abutments. This can be explained by that the CMEJ restrains the relative displacement between the abutment

and the girder once tightened; the inertial force of the superstructure is thus partially transmitted to the abutment, and the seismic response of the abutment increases while the bearing deformation decreases. Due to the sliding of LRBs, the expected repair cost and the damage probability of bridge piers are negligible, which agrees with previous studies [46]. In general, the total expected repair cost for the bridge with CMEJ is decreased by 77.8 %, which indicates the seismic resistance system is effective in improving the seismic performance.

Numerical models with 0° , 15° , 45° , 60° skew angles are also developed for parametric study. The second-order polynomial regres-

Table 7

Optimum design parameters and expected repair cost for different bridge cases.

Cases	Optimum design parameter A_B (m^2)	t_R (m)	Δ_J (m)	$F(X)$ by RSM (\$)	$F(X)$ by NS (\$)	$E[L_c X]$ by NS(\$)	$E[L_T X]$ by NS (\$)		
					Bearing	Pier	Abutment		
0°-MEJ	0.18	0.09	0.05	1,284,168	1,253,003	46,141	7418	54,196	
0°-CMEJ	0.18	0.09	0.05	1,179,289	1,198,807	10,742	550	10,864	22,155
15°-MEJ	0.18	0.09	0.05	1,269,288	1,275,741	69,249	648	7036	76,934
15°-CMEJ	0.18	0.09	0.05	1,179,185	1,220,787	10,543	606	10,831	21,980
30°-MEJ	0.18	0.09	0.05	1,306,228	1,302,787	96,504	884	6592	103,980
30°-CMEJ	0.18	0.09	0.05	1,182,550	1,221,931	12,062	632	10,430	23,124
45°-MEJ	0.18	0.09	0.05	1,335,763	1,321,913	115,715	1216	6174	123,106
45°-CMEJ	0.18	0.09	0.05	1,179,423	1,221,177	13,216	771	8384	22,370
60°-MEJ	0.18	0.09	0.05	1,332,943	1,333,413	127,245	1347	6014	134,606
60°-CMEJ	0.18	0.09	0.05	1,183,838	1,221,987	12,071	631	10,478	23,180

sion results of the RSM are summarized in Table 6. The optimal design parameters and expected repair cost by numerical simulation (NS) corresponding to various skew angles are shown in Table 7. In terms of repair cost estimation, $E[L_T|X]$ of the bridge with MEJs increases with increasing of skew angles, as the rotation response is increased. The total expected repair cost of the bridge with CMEJ is independent of skew angles. Moreover, errors of the objective function between the numerical simulation and RSM are within 4 % for all cases, proving that the accuracy of RSM is acceptable for the optimization of the cost-related objective function.

9. Conclusions

This paper investigates the design and optimization of the earthquake-resistant system for continuous skew overpasses. The contents of this study mainly include: (1) modified probabilistic seismic demand model (PSDM) based on BOX-COX regression; (2) selection of the optimal intensity measure (IM) out of ten IM candidates for the PSDM. (3) probabilistic seismic loss assessment during the bridge life cycle; (4) optimization framework to determine the optimal design parameters for the earthquake-resistant system with a cost-related objective function; (5) evaluation of the seismic mitigation effectiveness of the cable-sliding modular expansion joint (CMEJ). Conclusions are drawn as follows:

- The BOX-COX regression can improve the linearity, normality, and homoskedasticity of the PSDM. When all three assumptions of the cloud method are satisfied, identical PSDMs are obtained using both the cloud method and the modified method.
- Based on the criteria of efficiency, practicality, proficiency, correlation, and sufficiency, PGV, VSI, and S_{a-10} show better performance compared to acceleration-related IMs and displacement-related IMs. Particularly, S_{a-10} is selected as the optimal IM considering hazard computability and is used for the probabilistic seismic loss assessment of the example bridge.
- The optimization procedure is viable to determine the optimal design parameters for the earthquake-resistant system efficiently with a cost-related objective function, where the function consists of construction cost and expected seismic repair cost. The errors of the objective function between the numerical simulation and response surface method (RSM) are less than 4 %.
- Compared to the bridge with MEJs, bearings of the bridge with CMEJs retain less damage probability, while the damage probability of abutments increases, which results in the total expected repair cost decreasing by 77.8 %.
- Due to the rotation of the bridge girder, the total expected repair cost of the bridge with MEJs increases as the skew angle becomes more extensive. After the CMEJ is adopted, the total expected repair cost of the bridge is independent of the skew angle.

Declaration of Competing Interest

The authors declare that they have no known competing financial interests or personal relationships that could have appeared to influence the work reported in this paper.

Acknowledgment

This research was supported by the National Key Research and Development Program of China No. 2021YFF0502200; the National Natural Science Foundation of China under Grant No. 51978511, 51778470, 52008316; Science and Technology Commission of Shanghai Municipality No. 20ZR1461400 (Natural Science Foundation), 20PJ1413900 (Shanghai Pujiang Program). Special thanks to Dr. Ruiwei Feng, Dr. Junjun Guo, Mr. Lianxu Zhou, and Ms. Juanya Yu for providing insightful suggestions and valuable assistance to this paper. Dedicated to the memory of Dr. Wancheng Yuan (1962-2022).

References

- [1] Han Q, Du X, Liu J, Li Z, Li L, Zhao J. Seismic damage of highway bridges during the 2008 Wenchuan earthquake. *Earthq Eng Eng Vib* 2009;8:263–73.
- [2] Buckle I, Hube M, Chen G, Yen W-H, Arias J. Structural performance of bridges in the offshore Maule earthquake of 27 February 2010. *Earthq Spectra* 2012;28: 533–52.
- [3] Kawashima K, Unjoh S, Hoshikuma J-I, Kosa K. Damage of bridges due to the 2010 Maule, Chile, earthquake. *J Earthq Eng* 2011;15:1036–68.
- [4] Kwon O-S, Jeong S-H. Seismic displacement demands on skewed bridge decks supported on elastomeric bearings. *J Earthq Eng* 2013;17:998–1022.
- [5] Maleki S, Bagheri S. Seat width requirement for skewed bridges under seismic loads. *Sci Iran* 2014;21:1471–9.
- [6] Wu S. Unseating mechanism of a skew bridge with seat-type abutments and a Simplified Method for estimating its support length requirement. *Eng Struct* 2019; 191:194–205.
- [7] Wu S, Buckle IG. Effect of skew on the minimum support length requirements of single-span bridges with seat-type abutments. *Earthq Spectra* 2020;36:1119–40.
- [8] Sevgili G, Caner A. Improved seismic response of multispan skewed bridges retrofitted with link slabs. *J Bridg Eng* 2009;14:452–9.
- [9] Watabane G, Kawashima K. Effectiveness of cable-restrainer for mitigating rotation of a skewed bridge subjected to strong ground shaking. *13th World Conf Earthq Eng Vancouver* 2004:1–14.
- [10] Saiedi M, Randall M, Maragakis E, Isakovic T. Seismic restrainer design methods for simply supported bridges. *J Bridg Eng* 2001;6:307–15.
- [11] Gao K, Yuan W, Cao S, Pang Y. Seismic performance of cable-sliding modular expansion joints subject to near-fault ground motion. *Lat Am J Solids Struct* 2015; 12:1397–414.
- [12] Gao K, Yuan WC, Dang XZ. Development and experimental study on cable-sliding modular expansion joints. *Struct Eng Mech An Int J* 2017;61:795–806.
- [13] Zhang P, Feng R, Zhou L, Guo J, Yuan W. Seismic fragility analysis of skew bridges with cable-slide modular expansion joints. *J Tongji Univ* 2021;49:816–24.
- [14] Sung Y-C, Su C-K. Fuzzy genetic optimization on performance-based seismic design of reinforced concrete bridge piers with single-column type. *Optim Eng* 2010;11: 471–96.
- [15] Nigdeli SM, Bekdaş G, Alhan C. Optimization of seismic isolation systems via harmony search. *Eng Optim* 2014;46:1553–69.
- [16] Xu Z-D, Guo Y-F, Wang S-A, Huang X-H. Optimization analysis on parameters of multi-dimensional earthquake isolation and mitigation device based on genetic algorithm. *Nonlinear Dyn* 2013;72:757–65.
- [17] Moendarbari H, Taghikhany T. Novel procedure for reliability-based cost optimization of seismically isolated structures for the protection of critical

- equipment: A case study using single curved surface sliders. *Struct Control Heal Monit* 2018;25:1–19.
- [18] Çerçevik AE, Avşar Ö, Hasançebi O. Optimum design of seismic isolation systems using metaheuristic search methods. *Soil Dyn Earthq Eng* 2020;131:106012.
- [19] Zhang J, Huo Y. Evaluating effectiveness and optimum design of isolation devices for highway bridges using the fragility function method. *Eng Struct* 2009;31: 1648–60.
- [20] Hu S, Zou Y, Gai Y, Huang Z, Song G. Risk-based multiobjective optimal seismic design for RC piers using the response surface method and NSGA-II. *Adv Civ Eng* 2021;2021:1–11.
- [21] Karalar M, Padgett JE, Dicleli M. Parametric analysis of optimum isolator properties for bridges susceptible to near-fault ground motions. *Eng Struct* 2012; 40:276–87.
- [22] Hu S, Chen B, Song G, Wang L. Resilience-based seismic design optimization of highway RC bridges by response surface method and improved non-dominated sorting genetic algorithm. *Bull Earthq Eng* 2022;20:449–76.
- [23] Idels O, Lavan O. Performance-based seismic retrofitting of frame structures using negative stiffness devices and fluid viscous dampers via optimization. *Earthq Eng Struct Dyn* 2021;50:3116–37.
- [24] Xie Y, Zhang J. Design and optimization of seismic isolation and damping devices for highway bridges based on probabilistic repair cost ratio. *J Struct Eng* 2018;144: 4018125.
- [25] Lee T-H. Probabilistic seismic evaluation of reinforced concrete structural components and systems. Berkeley: University of California; 2005.
- [26] Kameshwar S, Padgett JE. Characterizing and predicting seismic repair costs for bridges. *J Bridg Eng* 2017;22:04017083.
- [27] Shafeezaeh A, DesRoches R, Rix GJ, Werner SD. A probabilistic framework for correlated seismic downtime and repair cost estimation of geo-structures. *Earthq Eng Struct Dyn* 2014;43:739–57.
- [28] Mackie KR, Wong J, Stojadinović B. Post-earthquake bridge repair cost and repair time estimation methodology. *Earthq Eng Struct Dyn* 2010;39:281–301.
- [29] Mander JB, Dhakal RP, Mashiko N, Solberg KM. Incremental dynamic analysis applied to seismic financial risk assessment of bridges. *Eng Struct* 2007;29: 2662–72.
- [30] Ghosh J, Padgett JE. Probabilistic seismic loss assessment of aging bridges using a component-level cost estimation approach. *Earthq Eng Struct Dyn* 2011;40: 1743–61.
- [31] Nielson BG, DesRoches R. Seismic fragility methodology for highway bridges using a component level approach. *Earthq Eng Struct Dyn* 2007;36:823–39.
- [32] Muntasir Billah AHM, Shahria AM. Seismic fragility assessment of highway bridges: a state-of-the-art review. *Struct Infrastruct Eng* 2015;11:804–32.
- [33] Baker JW. Probabilistic structural response assessment using vector-valued intensity measures. *Earthq Eng Struct Dyn* 2007;36:1861–83.
- [34] Mackie K, Stojadinovic B. Relation between probabilistic seismic demand analysis and incremental dynamic analysis. 7th US Natl. Conf Earthq Eng 2002:21–5.
- [35] Karamlou A, Bocchini P. Quantification of the approximations introduced by assumptions made on marginal distributions of the demand for highway bridge fragility analysis. Second Int. Conf. vulnerability risk Anal. Manag. (ICVRAM 2014), 2014, p. 1321–30.
- [36] Guo J, Zhong J, Dang X, Yuan W. Influence of Multidirectional Cable Restrainer on Seismic Fragility of a Curved Bridge. *J Bridg Eng* 2019;24:04019001.
- [37] Wang X, Shafeezaeh A, Ye A. Optimal intensity measures for probabilistic seismic demand modeling of extended pile-shaft-supported bridges in liquefied and laterally spreading ground. *Bull Earthq Eng* 2018;16:229–57.
- [38] Padgett JE, Nielson BG, DesRoches R. Selection of optimal intensity measures in probabilistic seismic demand models of highway bridge portfolios. *Earthq Eng Struct Dyn* 2008;37:711–25.
- [39] Du A, Padgett JE, Shafeezaeh A. A posteriori optimal intensity measures for probabilistic seismic demand modeling. *Bull Earthq Eng* 2019;17:681–706.
- [40] Zhong J, Jeon J-S, Shao Y-H, Chen L. Optimal intensity measures in probabilistic seismic demand models of cable-stayed bridges subjected to pulse-like ground motions. *J Bridg Eng* 2019;24:04018118.
- [41] Guo J, jun, Zhong J, Dang X zhi, Yuan W cheng.. Seismic performance assessment of a curved bridge equipped with a new type spring restrainer. *Eng Struct* 2017; 151:105–14.
- [42] Deng J, Hu F, Ozbulut OE, Cao S. Verification of multi-level SMA/lead rubber bearing isolation system for seismic protection of bridges. *Soil Dyn Earthq Eng* 2022;161:107380.
- [43] Box GEP, Cox DR. An analysis of transformations. *J R Stat Soc Ser B* 1964;26: 211–43.
- [44] Cornell CA, Jalayer F, Hamburger RO, Foutch DA. Probabilistic basis for 2000 SAC federal emergency management agency steel moment frame guidelines. *J Struct Eng* 2002;128:526–33.
- [45] Ramanathan K, DesRoches R, Padgett JE. A comparison of pre-and post-seismic design considerations in moderate seismic zones through the fragility assessment of multispan bridge classes. *Eng Struct* 2012;45:559–73.
- [46] Xiang N, Li J. Effect of exterior concrete shear keys on the seismic performance of laminated rubber bearing-supported highway bridges in China. *Soil Dyn Earthq Eng* 2018;112:185–97.
- [47] Revell J. Quasi-isolated highway bridges: influence of bearing anchorage strength on seismic performance. University of Illinois at Urbana-Champaign; 2013.
- [48] Fazli H, Pakbaz A. Performance-based seismic design optimization for multi-column RC bridge piers, considering quasi-. *Int J Optim Civ Eng* 2018;8:525–45.
- [49] Aslani H. Probabilistic earthquake loss estimation and loss disaggregation in buildings. Stanford University; 2005.
- [50] FEMA-227.. A benefit-cost model for the seismic rehabilitation of buildings. Washington, D.C.: Federal Emergency Management Agency; 1992.
- [51] Bradley BA, Dhakal RP, Cubrinovski M, Mander JB, MacRae GA. Improved seismic hazard model with application to probabilistic seismic demand analysis. *Earthq Eng Struct Dyn* 2007;36:2211–25.
- [52] JT/T 4-2019 Laminate bearing for highway bridge. China: Ministry of Transportation, People's Republic of China; 2019.
- [53] Nielson BG, Pang WC. Effect of ground motion suite size on uncertainty estimation in seismic bridge fragility modeling. *Struct Congr* 2011;2011:23–34.
- [54] Box GEP, Wilson KB. On the experimental attainment of optimum conditions. *Break Stat* 1992;270–310.
- [55] Towashiraporn P. Building seismic fragilities using response surface metamodels. Georgia Institute of Technology; 2004.
- [56] Kennedy J, Eberhart R. Particle swarm optimization. In: Proc ICNN'95-Int Conf Neural Netw, 4. IEEE; 1995. p. 1942–8.
- [57] Japanese JRA. Design specifications for highway bridges, Part V: Seismic design. Japanese: Japan Road Associa; 2012.
- [58] Mander JB, Priestley MJN, Park R. Theoretical stress-strain model for confined concrete. *J Struct Eng* 1988;114:1804–26.
- [59] JTG 3363-2019 Specifications for design of foundation of highway bridges and culverts. China: Ministry of Transportation, People's Republic of China; 2019.
- [60] Nielson BG. Analytical fragility curves for highway bridges in moderate seismic zones. Georgia Institute of Technology; 2005.
- [61] Kaviani P, Zareian F, Taciroglu E. Seismic behavior of reinforced concrete bridges with skew-angled seat-type abutments. *Eng Struct* 2012;45:137–50.
- [62] Lveqin X, Jianzhong L. Design and experimental investigation of a new type sliding retainer and its efficacy in seismic fortification. *Eng Mech* 2016;33:111–8.
- [63] Muthukumar S. A contact element approach with hysteresis damping for the analysis and design of pounding in bridges. Georgia Institute of Technology; 2003.
- [64] Li H, Li L, Zhou G, Xu L. Effects of various modeling uncertainty parameters on the seismic response and seismic fragility estimates of the aging highway bridges. *Bull Earthq Eng* 2020;18:6337–73.
- [65] Liu P-L, Der Kiureghian A. Multivariate distribution models with prescribed marginals and covariances. *Probabilistic Eng Mech* 1986;1:105–12.
- [66] JTG 3362-2018 Specifications for Design of Highway Reinforced Concrete and Prestressed Concrete Bridges and Culverts. China: Ministry of Transportation, People's Republic of China; 2018.
- [67] Barbatto M, Asce AM, Gu Q, Asce AM, Conte JP, Asce M. Probabilistic Push-Over Analysis of Structural and Soil-Structure Systems. *J Struct Eng* 2010;136:1330–41.
- [68] Le C, Wang Shuli WZ. Calibration of the steel strength standard value and the partial coefficient. *Constr Qual* 2012;61–5.
- [69] Stefanidis SP, Kappos AJ. Methodology for the development of bridge-specific fragility curves. *Earthq Eng Struct Dyn* 2017;46:73–93.
- [70] Mangalathu S, Heo G, Jeon JS. Artificial neural network based multi-dimensional fragility development of skewed concrete bridge classes. *Eng Struct* 2018;162: 166–76.
- [71] Pan Y, Agrawal AK, Ghosh M. Seismic fragility of continuous steel highway bridges in New York State. *J Bridg Eng* 2007;12:689–99.
- [72] Taskari O, Sextos A. Probabilistic assessment of abutment-embankment stiffness and implications in the predicted performance of short bridges. *J Earthq Eng* 2015; 19:822–46.
- [73] Baker JW, Lee C. An improved algorithm for selecting ground motions to match a conditional spectrum. *J Earthq Eng* 2018;22:708–23.
- [74] Boore DM, Stewart JP, Seyhan E, Atkinson GM. NGA-West2 equations for predicting PGA, PGV, and 5% damped PSA for shallow crustal earthquakes. *Earthq Spectra* 2014;30:1057–85.
- [75] Priestley MJN, Seible F, Calvi GM. Seismic design and retrofit of bridges. John Wiley & Sons; 1996.
- [76] Feng R, Yuan W, Sextos A. Probabilistic loss assessment of curved bridges considering the effect of ground motion directionality. *Earthq Eng Struct Dyn* 2021;1–23.
- [77] Spearman SC. The Proof and measurement of association between two things. *Am J Psychol* 1904;15:72–101.
- [78] Zar JH. Significance testing of the spearman rank correlation coefficient. *J Am Stat Assoc* 1972;67:578–80.